2013

Activity Intent Recognition of the Torso Based on Surface Electromyography and Inertial Measurement Units

Zhe Zhang
University of Massachusetts Amherst

**ACTIVITY INTENT RECOGNITION OF THE TORSO BASED ON SURFACE
ELECTROMYOGRAPHY AND INERTIAL MEASUREMENT UNITS**

A Thesis Presented

by

ZHE ZHANG

Submitted to the Graduate School of the
University of Massachusetts Amherst in partial fulfillment
of the requirements for the degree of

MASTER OF SCIENCE IN MECHANICAL ENGINEERING

May 2013

Department of Mechanical and Industrial Engineering

ACTIVITY INTENT RECOGNITION OF THE TORSO BASED ON SURFACE ELECTROMYOGRAPHY AND INERTIAL MEASUREMENT UNITS

A Thesis Presented

by

ZHE ZHANG

Approved as to style and content by:

_____

Frank C Sup, Chair

_____

Yossi Chait, Member

_____

Yahya Modarres-Sadeghi, Member

_____

Donald Fisher, Department Head

Department of Mechanical and Industrial

Engineering

ACKNOWLEDGMENTS

First, I would like to record my gratitude to my advisor, Professor Frank Sup, for all of his patient support, guidance, and encouragement throughout my time working for him as a graduate student. He has been an invaluable asset to my continued education of mechatronics and robotics outside of the classroom, as well as a great source of inspiration and motivation that I will take with me well past my days as a student. I'd also like to thank my thesis defense committee members, Profs Yossi Chait and Yahya Modarres-Sadeghi for their feedback and contributions to my thesis project. They too have been a great source of inspiration, guidance and knowledge throughout my years as a student.

Many thanks go to everyone I've worked with in the Mechatronics and Robotics Research Laboratory and the Kinesiology Biomechanics Laboratory. Lastly, I would like to thank my family for all their love and encouragement. For my parents who raised me with full of love and supported me in all my pursuits.

ABSTRACT

INTENT ACTIVITY MODE RECOGNITION BASED ON SURFACE

ELECTROMYOGRAPHY AND INERTIAL MEASUREMENT UNIT

MAY 2013

ZHE ZHANG, B.S., BEIJING JIAOTONG UNIVERSITY

M.S.M.E., UNIVERSITY OF MASSACHUSETTS AMHERST

Directed by: Professor Frank Sup

This thesis presents an activity mode intent recognition approach for safe, robust and reliable control of powered backbone exoskeleton. The thesis presents the background and a concept for a powered backbone exoskeleton that would work in parallel with a user. The necessary prerequisites for the thesis are presented, including the collection and processing of surface electromyography signals and inertial sensor data to recognize the user's activity. The development of activity mode intent recognizer was described based on decision tree classification in order to leverage its computational efficiency. The intent recognizer is a high-level supervisory controller that belongs to a three-level control structure for a powered backbone exoskeleton. The recognizer uses surface electromyography and inertial signals as the input and CART (classification and regression tree) as the classifier. The experimental results indicate that the recognizer can extract the user's intent with minimal delay. The approach achieves a low recognition

error rate and a user-unperceived latency by using sliding overlapped analysis window. The approach shows great potential for future implementation on a prototype backbone exoskeleton.

TABLE OF CONTENTS

LIST OF TABLES

LIST OF FIGURES

CHAPTER 1

INTRODUCTION

Recent technological advances in robotics make possible the development of an exoskeleton that can act as an extension of themselves. Augmenting the upper and lower limbs has been the primary focus of exoskeleton research to-date. A powered backbone component of an exoskeleton can increase the load carrying capacity of a person and can potentially benefit a wide array of people, ranging from people bringing groceries into their homes, to people suffering from disabilities such as: paraplegia and hemiplegia, since daily activities such as flexion or extension can prove to be very challenging for them. In these respective cases, the benefits could result in improved load carrying capacity and an ability to stand and walk freely. By making the control of the device intuitive, the user needs to worry less about its operation and can be more concerned about participating in activities of daily life. But current exoskeleton technology still limits the natural flexibility and movement of the torso, the capabilities of users, and activities that users are able to participate in since the connection between the upper and lower limbs has been a rigid spine. In addition, when unintended events occur such as stepping on a rock or curb, maintaining ones balance and stability may be impossible.

1.1   Research objective

The objective of this research is to develop an intelligent, powered backbone exoskeleton with a real-time intent recognition system. The powered backbone exoskeleton has a three-level control structure which consists of a high-level supervisory controller, a middle-level controller and a low-level controller. This thesis will focus on the activity mode intent recognizer, which is a high-level supervisory controller and its function is to distinguish between the intent activities modes of subject, such as flexion, extension and twisting. The recognizer uses surface electromyography and inertial signals as the input and CART (classification and regression tree) as the classifier.

1.2   Research approach

The major goal of this research is to develop an intent recognition system for a powered backbone exoskeleton. To meet the final goal of this project, the project has been divided into two main sections, the first section is to develop concept for the mechanical structure of backbone exoskeleton and the second section focuses on the developing the intent recognition system. The research tasks are as follows.

1.   Understand the structure and mechanics of the human spine.

2.   Develop concept of a powered backbone exoskeleton.

3.   Develop an approach to collect surface electromyography signals and inertial signals.

4. Preprocess the raw signal by filtering, rectification and normalization. Extract signal feature by sliding window and reduce the data dimension by PCA.

5. Evaluate classifiers for intent recognition and filter out the noise by majority voting to determine the patient's intended activity and discuss the result.

Dividing the research into several steps can help to keep the project focused and easy to implement, which is important for the successful completion of project. The long term goal of this research is to develop an intelligent, intuitive powered backbone exoskeleton.

1.3   Scope

The project deliverables include a concept for a backbone exoskeleton and an appropriate intent recognition system for control of the device. This thesis will focus on the development of activity mode intent recognizer, which is a high-level supervisory controller and its function is to distinguish between the intent activity modes of subject, such as flexion, extension and twisting. The recognizer uses sEMG and inertial signals as the input and decision tree as the classifier. Designing an intelligent backbone exoskeleton involves the coordination of many tasks and attaining the help from many people in order to achieve the final goal. The project was implemented at the Mechatronics and Robotics Research Laboratory at the University of Massachusetts, Amherst and directed by Professor Frank Sup. Also attained help from the Biomechanics

Laboratory of the Kinesiology Department at the University of Massachusetts, Amherst for the instruction of human torso biomechanics and neural-muscular system.

1.4   Structure of this thesis

This thesis is organized into six chapters. After introduction, Chapters 2 presents the design concept of backbone exoskeleton which would provide scientific insights into the effects of an external flexible robot on the human backbone. Chapter 3 describes the background of electromyography signal, which includes the history and physiology of EMG signal, and also the collection, processing and application of EMG signal. Chapter 4 introduces the basic knowledge of pattern recognition and the background of decision tree classification. Chapter 5 describes the detailed procedure for surface electromyography and inertial signals based activity mode intent recognition, and discuss the result of experiments. In chapter 6, conclusions from the work are presented and along with suggestions for further improvement. In Appendix, the detailed recognition error rates results for the additional four subjects using different window lengths are presented.

CHAPTER 2

BACKGROUND OF BACKBONE EXOSKELETON

2.1 Introduction

An understanding of the dynamics of the human backbone is essential to modeling and designing such a powered exoskeleton device, targeted at the backbone. This can be achieved through experimental studies on simulated backbone devices. This work will help advance the knowledge related to strength augmenting devices and can help realize a functional powered backbone exoskeletons. This chapter aims to design and prototype an experimental test-bed that would provide scientific insights into the effects of an external flexible robot on the human backbone.

Research exoskeletons have been focused on power augmentation for the lower limbs, like the Berkeley Lower Extremity Exoskeleton (BLEEX) [1], [2], a quasi-passive leg exoskeleton from MIT [3], Hybrid Assisted Leg (HAL-3) [4] [5], or to all the four limb such as HAL-5 [6], Wearable Energetically Autonomous Robot (WEAR) and XOS by Raytheon [7] and Body Extender [8], etc. Besides, some other exoskeleton includes: A powered knee brace called RoboKnee [9] that functions in parallel to the wearer's knee but does not transfer loads to the ground. This device transfers the weight of the load onto the human skeleton (including shanks, ankles, and feet), a joint-coupled controlled brake orthosis (JCO) [10] has been designed as part of a hybrid FES/orthosis system for

restoring gait to spinal cord injured individuals, a rehabilitation system Lokomat [11] where the patient legs are driven by the device through a predefined trajectory without any feedback from the patient. Below is more detail information about two excellent exoskeleton projects: Berkeley Lower Extremity Exoskeleton (BLEEX) and Hybrid Assistive Leg (HAL-5).

The Berkeley Lower Extremity Exoskeleton (BLEEX) was the first functional load-carrying and energetically autonomous exoskeleton. Users were able to walk at an average speed of 1.3 m/s while carrying a 34 kg (75 lb) payload. Four essential technologies were tackled during the course of this project include: the exoskeleton architecture design, control schemes, a body local area network (bLAN) to host the control algorithm and an on-board power unit to power the sensors, actuators and the computers. BLEEX allows the pilot to comfortably finish some basic daily motions such as: flexion and extension of the spine, twisting left or right, swing from side to side and walk on ascending and descending slopes, while also offering the ability to step over and under obstructions while carrying payload (equipment or supplies). The BLEEX has a wide potential application area include: it can provide disaster relief workers, soldiers, fire fighters and other emergency personnel the ability to carry heavy loads such as food, first-aid supplies, rescue equipment, communications gear and weaponry. Fig.1 gives us the system overview of BLEEX.

Figure 1. Berkeley Lower Extremity Exoskeleton (BLEEX) and pilot. [1]
1: Load occupies the upper portion of the backpack and around the Power Unit; 2: Rigid connection of the BLEEX spine to the pilot's vest; 3: Power unit and central computer occupies the lower portion of the backpack; 4: Semi-rigid vest connecting BLEEX to the pilot; 5: One of the hydraulic actuators; 6: Rigid connection of the BLEEX feet to the pilot's boots.

Hybrid Assistive Leg (HAL-5) is a robotics suite developed by University of Tsukuba, which is integrated with human and helps lower limb of people with gait disorder, provide a way for them to be able to continue walking without assistance from a caregiver, in order to prevent them from becoming bedridden. The exoskeleton system is constructed as master/slave system that master is incorporated into slave system. Using the exoskeleton as a master device in a master/slave system cables the operator attached to the exoskeleton (master) to control HAL-5 (slave) and to generate amplified power. HAL-5 system is consisted of three main parts: skeleton and actuator, controller, and sensor. Fig.2 gives us the whole system overview of HAL-5, which is currently being commercialized.

Figure 2. HAL-5 system overview. [6]

Each of these prior research works has their advantages and drawbacks, but all these devices provide power only to joints of arms and legs, none of them actuate back and torso. Moreover, the structures for the back and torso in these exoskeletons are rigid structures intended to either provided support or limit motion, and are limited to a central anchoring point in most cases. They cannot actively reduce the loading of the spine or augment its strength while maintaining its flexibility since these devices lack actuation. Among exoskeletons that focus on providing actuation to the back are an assistive device for lower back support [12], [13] and a wearable power assisting suit [14]. Both of these devices incorporate rigid links to provide assistive torque to the back, resulting in a rigid and straight posture. In each of these cases, the natural flexibility of the human spine is compromised. Overcoming the limitations imposed by absence of actuation and lack of

flexibility presents an avenue for the development of a fully active backbone exoskeleton that would provide strength augmentation during load carrying and benefit people suffering from spinal cord injuries.

The overall goal of the work that thesis contributes to is the development of a powered backbone exoskeleton that maintains the natural flexibility of the spine and also fulfill all the functions which an assistive device required at the same time. Fig.3 shows the HAL-5 exoskeleton spine [15], [16] which is a research thrust in a similar direction. Also, previous research on flexible links has been within the domain of flexible and continuum manipulators. More prominent in this field are hyper degree-of-freedom, rigid-link manipulators [17]. These manipulators are made up of an assembly of a large number of small, pin-jointed, rigid links that contribute to an immensely large number of degrees-of-freedom. The literature available in this field is exhaustive in nature, ranging from analysis of kinematics and dynamics, to design and control of manipulators arms [18–20]. Flexible, elastic (non-rigid) links and manipulators have also been widely researched, as can been seen from this review [21] and other related works [22], [23]. However, much of the work is very general in nature and cannot be easily adapted to our project. Therefore in this section, we describe our approach to this problem which models the structural members of the exoskeleton frame as an assembly of three elastically flexible sections connected by high-impedance revolute joints, and to design the rest of the exoskeleton components based on this frame [15].
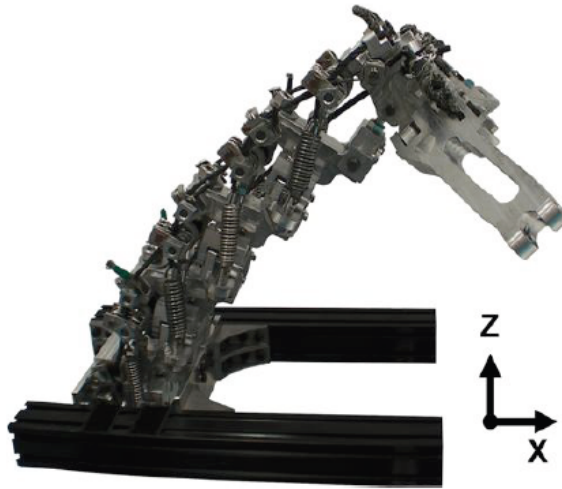
Figure 3. Exoskeleton spine for HAL-5.

2.2 Backbone exoskeleton design concept

The vertebral column in the human body consists of twenty-four articulating vertebrae in the cervical, thoracic and lumbar curves, and nine fused vertebrae in the sacral and coccygeal curves. The proposed exoskeleton is conceptualized to work with twenty-four articulate vertebrae in the cervical, thoracic and lumbar curves. The nine fused vertebrae of the coccygeal region are approximated in the fixed supports of the design.

A two-dimensional concept sketch of the exoskeleton structural frame is shown in Fig.4 (a). Two identical spines are installed side by side on a rigid platform and connected via mechanical linkages that represent a brace/corset. The left backbone designated as the internal backbone with a known weight, the right backbone designated as the exoskeleton. Alongside is a figure of a human backbone (Fig.4 (b)).
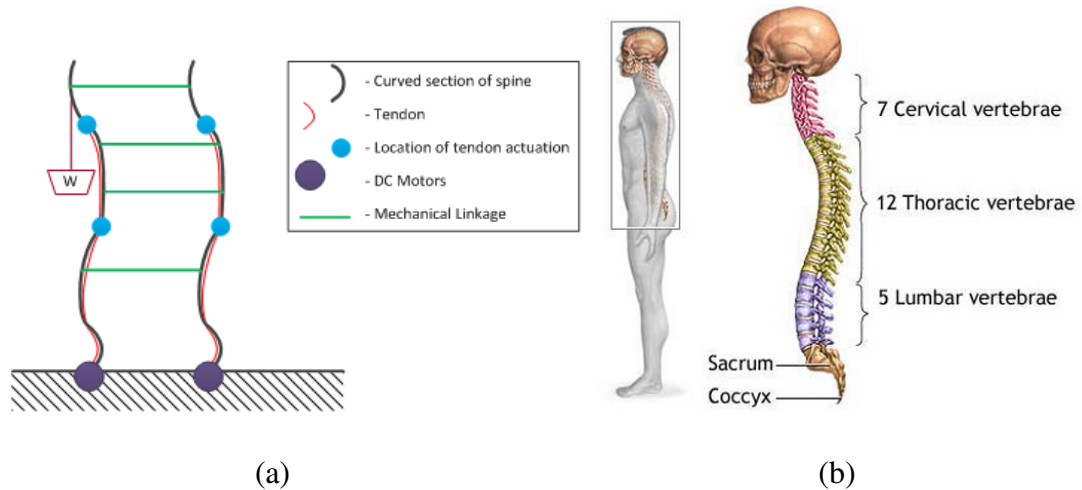
Figure 4. (a) Structural frame of backbone exoskeleton. (b) Human backbone. [24]

The structural frame of the exoskeleton is a manipulator consists of three flexible sections. Each section would be designed to represent and closely mimic the cervical, thoracic and lumbar segments of the human spine. The links of each section are to be assembled together via high-impedance revolute joints. These joints can help separate the individual curved segments and therefore helpful in controlling the curvature of individual segments. Actuation would be provided at three locations by three pairs of opposing tendons, driven by motors located at the base of the structure. The motors and tendons are configured in an overlapping manner. Specially, the cervical segment is subject to moments from a single motor. The thoracic segment in turn is designed to respond to moments from two motors and the lumbar segment is subject to moments from all three motors.

CHAPTER 3

BACKGROUND OF ELECTROMYOGRAPHY SIGNAL

3.1   History of Electromyography signal

In 1664, the beginning of research about electromyography (EMG) signal, Jan Swammerdam [25] discovered that stroking the innervating nerve of the frog's gastrocnemius generated a contraction and he also conducted the first electrical stimulation experiments. Luigi Galvani [25] is credited as the father of neurophysiology for his research work with frogs' legs, he showed that electrical stimulation of muscular tissue produces contraction and force. Francesco Redi [26] was the first scientist to recognize the connection between muscles and generation of electricity. Alessandro Volta [27] developed a device which produced electricity and could be used to stimulate muscles.

In 1838, Matteucci [25] used galvanometer (an instrument used to detect, measure, and determine the direction of small electric currents by means of mechanical effects produced by a current-carrying coil, designed by Carlo Matteucci) in a magnetic field to show that bioelectricity is connected with muscular contraction and in 1842 he demonstrated the existence of the action potential accompanying a frog's muscle.

The term electromyography comes from Etienne Marey, who modified Lippman's capillary electrometer (1876) as one of his many contributions to kinesiology. Willem Einthoven [25] made a string galvanometer in 1903 and won the Nobel Prize for it, it uses a thin conductor wire placed between two magnets. In 1922, Gasser and Erlanger used an oscilloscope to show the electrical signals from muscles, but because of the stochastic nature of the myoelectric signal, only rough information could be obtained from its observation. In 1929, Adrian and Bronk [28] developed the concentric needle electrode and used it primarily for researching motor control and muscle schemes. The capability of detecting electromyographic signals improved steadily from the 1930s through the 1950s and researchers began to use improved electrodes more widely for the study of muscles [29]. Clinical use of surface EMG (sEMG) for the treatment of more specific disorders began in the 1960s. Hardyck and his researchers were the first (1966) practitioners to use sEMG. In the early 1980s, Cram and Steger [30] introduced a clinical method for scanning a variety of muscles using an EMG sensing device. The most influential person in recent EMG history might be Carlo Luca, he wrote the famous often-cited paper: "The Use of Surface Electromyography in Biomechanics" [31].

3.2   Physiology of the EMG signal

3.2.1   Skeletal muscle organization

There are three kinds of muscles: skeletal muscles, heart muscle and smooth muscle. Skeletal muscles are the muscles attached to the skeleton and the only kind of muscles which can be controlled voluntarily by a person. The structure of skeletal muscle (Fig.5) includes: muscle fibers (wrapped by endomysium), muscle fascicles (bundles of muscle fibers, wrapped by perimysium) and attached to bones via tendons (composed of epimysium).
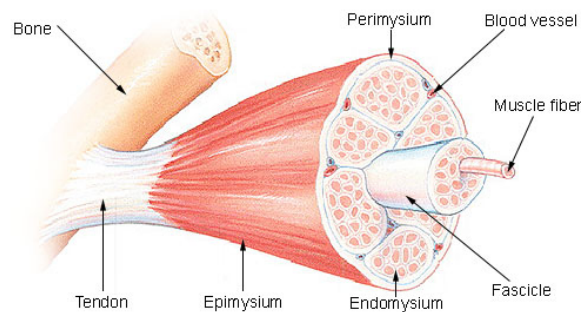
Figure 5. Skeletal muscle structure. [32]

3.2.2   Muscle contraction and the production of EMG signal

The contraction of skeletal muscles is controlled by the nervous system. Each muscle fiber can be recruited by one motor neuron. One motor neuron can branch in up to several thousand branches, each one terminating in a different muscle fiber. A motor neuron and all the fibers it innervates are called a motor unit (Fig.6).
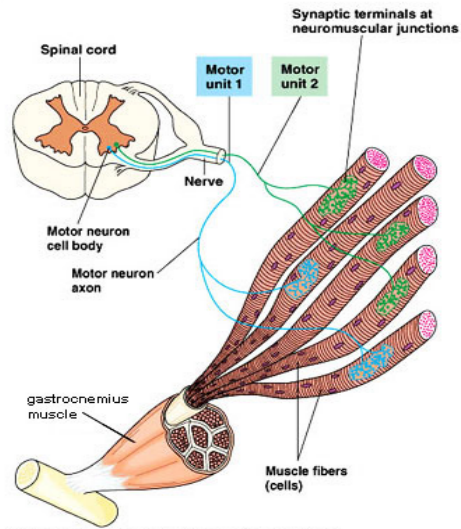
Figure 6. Typical motor unit. [33]

When a motor unit fires, the impulse (called an action potential) is carried down the motor neuron to the muscle. The area where the nerve contacts the muscle is called the neuromuscular junction, or the motor end plate. After the action potential is transmitted across the neuromuscular junction, an action potential is elicited in all of the innervated muscle fibers of that particular motor unit. The sum of all this electrical activity is known as a motor unit action potential (MUAP) and the sum of all independent MUAPT is the original EMG signal (Fig.7). This electrophysiological activity from multiple motor units is the signal typically evaluated during an EMG. The composition of the motor unit, the number of muscle fibers per motor unit, the metabolic type of muscle fibers and many other factors affect the shape of the motor unit potentials in the electromyogram.
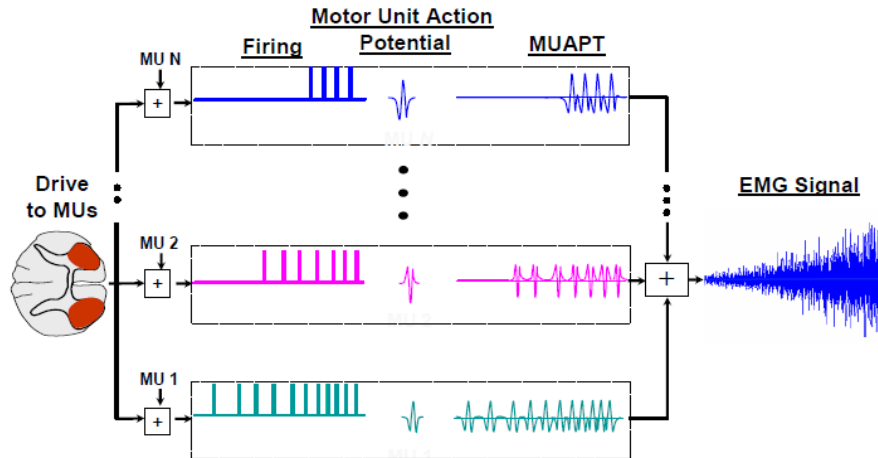
Figure 7. The composing of original EMG signal. [34]

3.3   Collection of EMG signal

Electrodes, amplifier and A/D converter were needed to collect raw EMG signal. Electrodes serve as converters of the ionic currents produced in muscles into electronic currents that can be manipulated in electronic circuits. Amplifier can optimize the resolution of the digitizing equipment. Besides, an amplifier can also be used to maximize the signal-to-noise ratio, that is, the ratio of the energy of the wanted EMG signal to the energy of unwanted noise contributions of the environment. A/D-converter transforms an analog signal into a discrete digital signal.

3.3.1   Electrodes

There are two main kinds of electrodes: inserted electrode (fine-wire or needle) and surface electrode (bipolar or array). Fig.8 shows variations on these kinds of

electrodes and each kind has advantages and disadvantages [35]. For inserted electrode, its advantages include: extremely sensitive, record the activity of a single motor unit, access to deep musculature and little cross-talk concern; disadvantages include: requires certification of medical personnel, repositioning nearly impossible and detection area may not be representative of entire muscle. For surface electrode, its advantages include: quick, easy to apply, no medical supervision and certification, minimal discomfort and easy to reposition; disadvantages include: generally used only for superficial muscles, cross-talk concerns, no standard electrode placement and may affect movement patterns of subject.

(a)   (b)

(c)   (d)
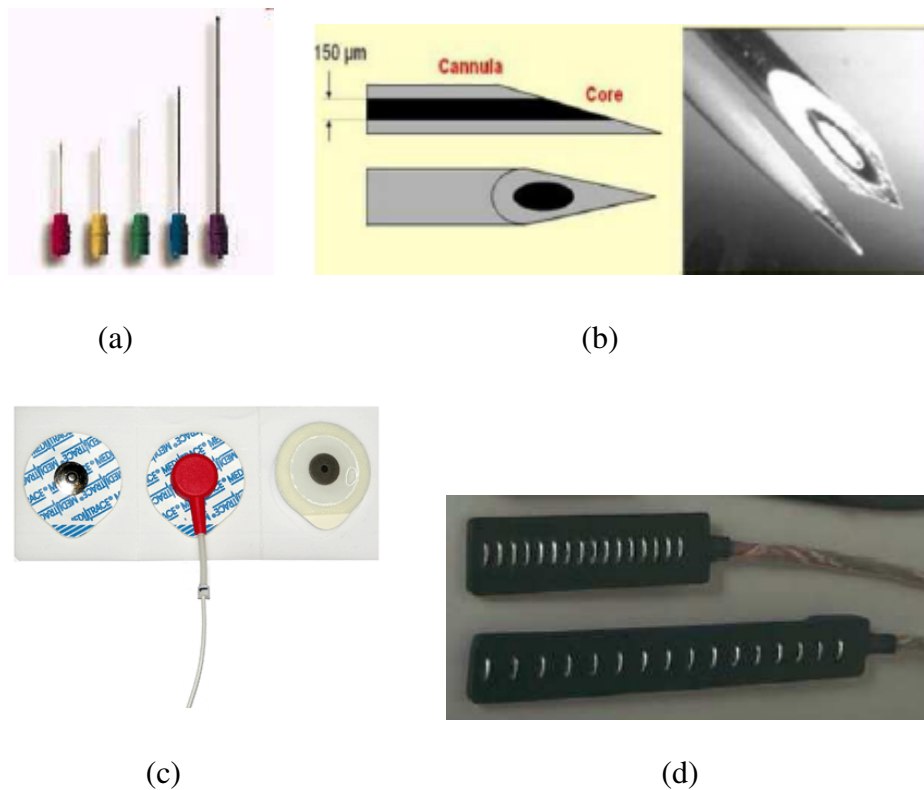
Figure 8. Different kinds of electrode.　(a) Fine-wire inserted electrode.　(b) Needle inserted electrode.　(c) Surface bipolar electrode.　(d) Surface array electrode.

In this project, surface array electrodes were chose for their simplicity, ease of application, subject comfort, no medical supervision needed, and detection area can be the representative of entire muscle. Compared to bipolar surface electrode, surface array electrodes can identify single MU action potentials (MUAPs) located at innervation and tendon zones, estimate conduction velocity (CV) of the individual MUAPs and of their firing patterns.

Fig.9 shows the geometry of DELSYS DE-2.3 single differential surface EMG sensor used in this project. The sensor housing is constructed from durable polycarbonate and completely sealed. It is also internally shielded to reject ambient electrical noise. Specialized signal conditioning circuitry ensures a noise-free, stable EMG signal with a full bandwidth of 20-450 Hz. The sensor contacts are made from 99.9% pure silver bars measuring 10mm in length, 1mm in diameter and spaced 10mm apart for optimal signal detection and consistency. The curved enclosure geometry (see Figure on the right) is designed to maximize skin contact and adhesion while minimizing the negative effects of sweat during vigorous activities.
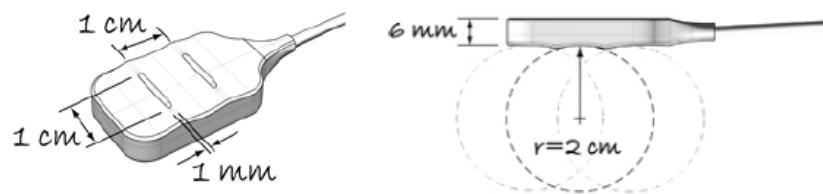
Figure 9. DELSYS DE-2.3 single differential surface EMG sensor geometry. [36]

3.3.2 Orienting and attaching the sEMG sensors on the skin

The DE-2.3 sEMG sensor is fitted with two silver bar contacts for detecting the EMG signal at the skin surface. It is crucial that the orientation of these bars be perpendicular to the muscle fibers for maximum signal detection (Fig.10). The top of the sensor is stamped with an arrow to aid in the determination of this orientation. The arrow should be placed parallel to the muscle fibers underneath the sensor. The sensor should also be placed in the center of the muscle belly away from tendons and the edge of the muscle.
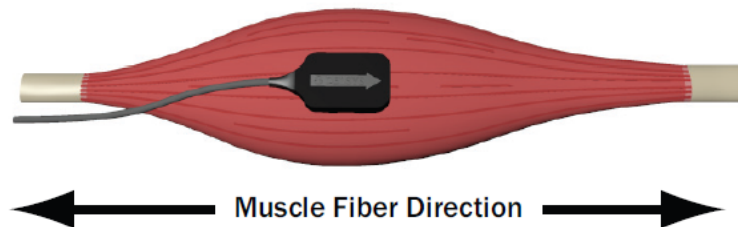
Figure 10. EMG sensor orientation with respect to the muscle fibers. [36]

The sensor is easily attached to the skin using the DELSYS Adhesive Sensor Interface. The Adhesive Sensor Interfaces use medical-grade adhesive specifically designed for dermatological applications. Usage of the interface promotes a high quality electrical connection between the sensor bars and the skin, minimizing motion artifacts and the ill-effects of line interference. To ensure a strong bond with the skin, the skin area

and the EMG sensors are wiped with isopropyl alcohol to remove oils and surface

residues. The skin was allowed to dry completely before application.

3.3.3   Surface EMG collection circuit

Surface EMG signals are very weak. Fig.11 shows an example of unamplified

sEMG signal and its corresponding frequency spectrum. The amplitude range is about

0-0.1 mV before amplification, frequency range is about 10-500 Hz but the dominant

energy focus on the range of 50-150 Hz, its peak appears at the range of 80-100 Hz.

Nyquist–Shannon sampling theorem tells us that the sampling frequency should be at

least two times of the signal highest frequency in order to prevent information from

losing, thus the sampling frequency should be at least 1000 Hz when collecting sEMG

signal based on the fact that the sEMG signal highest frequency component is around the

range of 400-500 Hz.
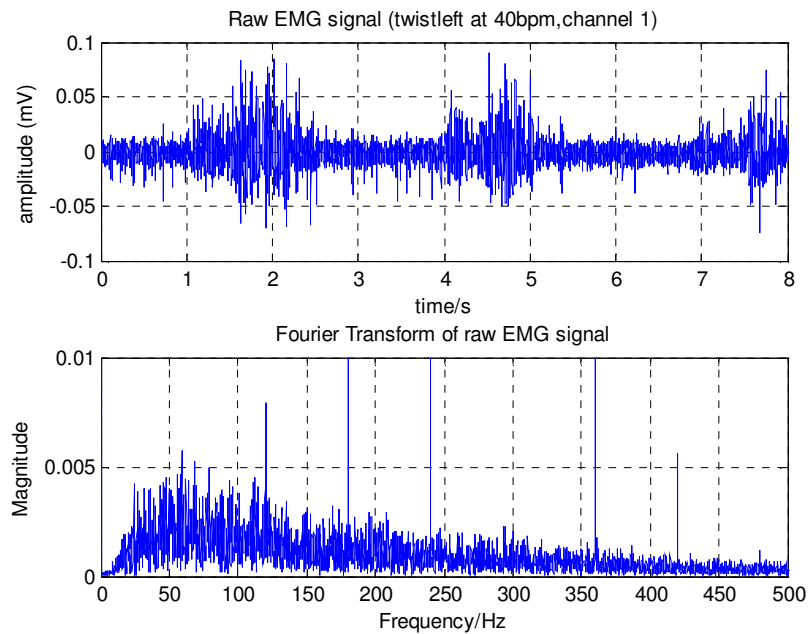
Figure 11. Example of an unamplified surface EMG signal and its corresponding frequency spectrum.

The quality of the detected sEMG signal determines the usefulness of the information extracted from the sEMG signal, it depends on: sensor location (upon the middle of muscle belly), sensor characteristics, and electrode-skin interface (The skin area and the EMG sensors are wiped with isopropyl alcohol to remove oils and surface residues. The skin was allowed to dry completely before application), cross-talk from other muscles and noise contamination.

Noise is defined as any unwanted signal collected with the wanted signal and should be removed. The main sources of noise and the ways of removing them include: Physiological Noise (e.g. EKG, EOG, respiratory signals, etc, reduced by proper positioning of the sensors), Ambient Noise (power line radiation (50 or 60 Hz), removed

by differential amplification), Baseline Noise (Electro-chemical noise from skin-electrode interface reduced by effective skin preparation), Movement Artifact Noise (movement of electrode with respect to the skin which can be reduced by effective skin preparation, proper fixation of the sensor to the skin and filtering).

Fig.12 shows the schematic diagram of DE-2.3 sEMG sensor circuit. Input signals come from two different points of muscle and they should be closed (usually 1 to 2 cm), electrode should be alignment with the direction of muscle fibers in order to increase the probability of detecting same signal, the ground electrode should be placed on electrically neutral (e.g. bony) tissue relatively far away from the detection site in order to serve as common reference to the differential input of the preamplifier. Then the two original EMG input signals were sent to differential amplifier, subtracted and amplified the difference there. Finally, the output signal will be sent to A/D converter.
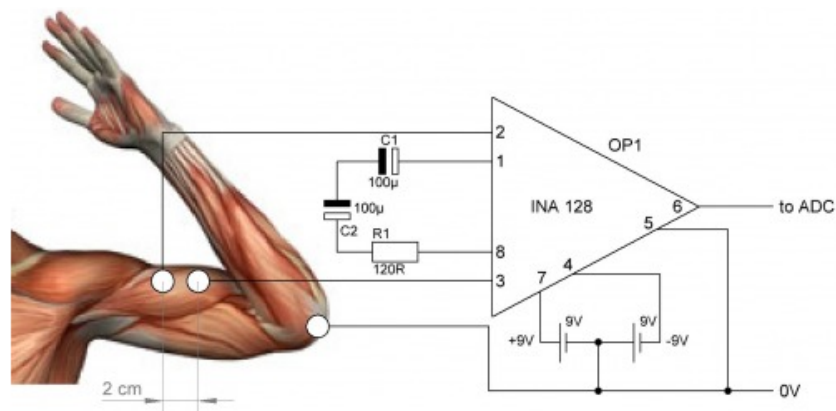
Figure 12. Schematic diagram of sEMG collection circuit. [37]
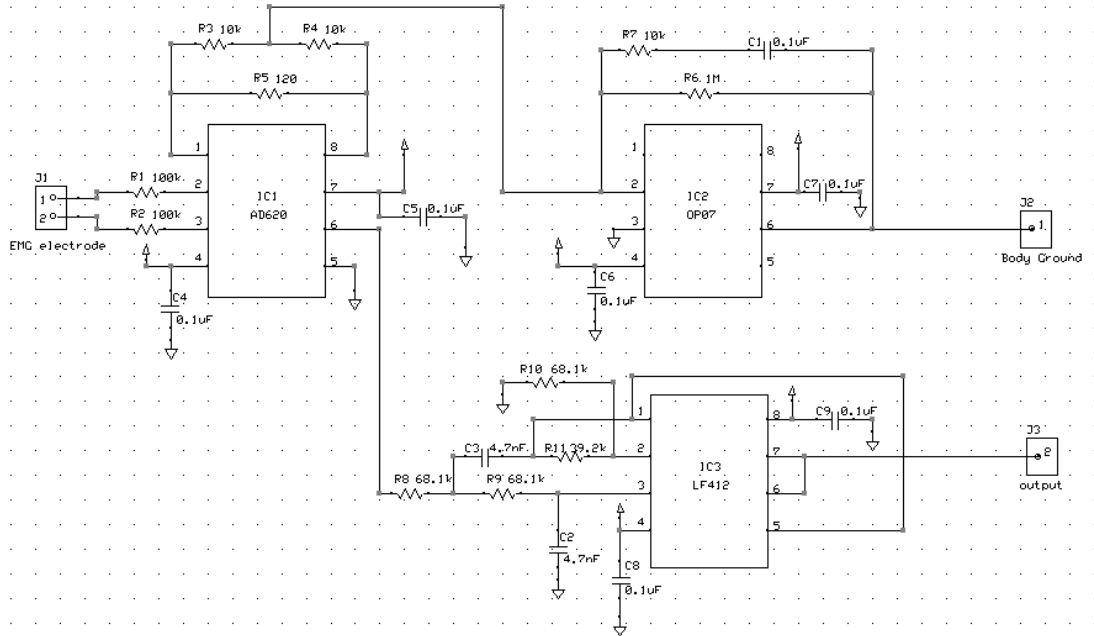
Figure 13. Complete sEMG collection circuit.

Fig.13 shows the complete sEMG collection circuit developed for this project. Instrumentation amplifier, Analog Devices AD620, were used and add a low pass filter circuit was added to remove the unwanted noise before sending the output signal to A/D converter. Fig.14 shows a complete commercial EMG measurement system suite (DELSYS Myomonitor IV Wireless EMG System), which is exactly what we use in our project for collecting sEMG signals.

Figure 14. sEMG system suite used for collecting muscle activity data (DELSYS Myomonitor IV Wireless sEMG System).

3.4   Processing of EMG signal

3.4.1   sEMG signal preprocessing

The raw sEMG signal has amplitude of 0-0.1 mV and frequency of 10-500 Hz, it represents the amount of muscle energy measured. Raw sEMG signals offer valuable information and must be processed to remove several types of artifacts. In this project, high-pass filtering, low-pass filtering, rectification and normalization were used for preprocessing.

3.4.2 sEMG signal feature extraction

The success of any pattern classification system significantly depends on the choice of features used to represent the raw signals. It is desirable to use multiple feature parameters for EMG pattern classification because it is difficult to extract a feature parameter which reflects the unique feature of the measured signals to a motion command perfectly. Considering some previous research works [38] [39] [40], the following four low computational cost features which could result in high classification accuracy rate based on time statistics are used in this project to represent the myoelectric pattern. Time domain features are calculated based on signal amplitude. They can be computed very fast since they don't need a signal transformation. All features are computed over a data segment with N samples.

1. Mean Absolute Value (MAV)

This is an estimate of mean absolute value of the signal, as defined by

$$\overline{x_i} = \frac{1}{N} \sum_{k=1}^{N} |x_k| \qquad (3.1)$$

where x_k is the kth sample in segment i.

2. Standard Deviation (SD)

This feature shows how much variation exists from the mean value of data segment, as defined by

$$s = \sqrt{\frac{1}{N}\sum_{i=1}^{N}(x_i - \bar{x})^2} \tag{3.2}$$

where $\bar{x}$ is the mean value of data segment.

3. Difference Absolute Mean Value (DAMV)

This is the mean absolute value of the difference between the adjacent samples, k and $k+1$, as defined by

$$\overline{\Delta x_i} = \frac{1}{N-1}\sum_{k=1}^{N-1}|x_{k+1} - x_k| \tag{3.3}$$

4. Root Mean Square (RMS)

Calculated by squaring each data point, summing the squares, dividing the sum by the number of observations and taking the square root, as defined by

$$RMS_k = \sqrt{\frac{1}{N}\sum_{i=1}^{N}x_i^2} \tag{3.4}$$

where it's a nth order AR model.

3.5 Applications of sEMG signal in rehabilitation engineering

sEMG signals are used in many clinical and biomedical applications. sEMG is used as a diagnostics tool for identifying neuromuscular diseases, assessing low-back pain and disorders of motor control. Especially, it can also be used for developing sEMG pattern recognition-based control approaches for powered prostheses. Some prior works such as: A Gaussian mixture model based classification scheme for myoelectric control of powered upper limb prostheses is described in [41]. A volitional control approach of a

prosthetic knee using surface electromyography is described in [42]. A multiclass real-time intent recognition method for a powered lower limb prosthesis is presented in [43]. Other researchers emphasize on describing the development of pattern recognition approach based on EMG signal, such as: An EMG-based pattern recognition approach for identifying locomotion modes by using artificial neural networks (ANN) and linear discriminant analysis (LDA) is presented in [44]. A robust, real-time control scheme for multifunction myoelectric control is presented in [45]. An EMG-based hand gesture recognition approach for real-time biosignal interfacing is described in [46].

Current prosthetic devices predominantly utilize sEMG signals from the user's body, in addition to pressure and force sensors, mounted at various locations on the device and along the body. Related prior research works such as: A multimodal interpretation of muscular activities using a body sensor network with electromyogram and inertial sensors is developed in [47]. An automatic recognition method of sign language sub-words based on portable accelerometer and EMG sensors is described in [48]. A rule-based control approach of walking by using decision trees and practical sensors is designed in [49].

CHAPTER 4

PATTERN CLASSIFICATION

4.1   Introduction

Pattern recognition in machine learning is the assignment of a label to a given input value. An example of pattern recognition is classification, which attempts to assign each input value to one of a given set of classes. Both choosing suitable feature parameters and a well-behaved classifier are important for EMG signal pattern recognition. Nowadays, with the fast development of the recognition theory, more and more different kinds of classifiers have been used for classifying sEMG signal. Below are some commonly-used classification methods:

1. *Statistical Pattern Classification*

It's very difficult to describe an EMG signal by mathematic function because of its random feature, but the statistical result indicates that the EMG signal has some statistical rules. Statistical pattern classification is an approach to machine intelligence which is based on statistical modeling of data. With a statistical model in hand, one applies probability theory and decision theory to get an algorithm. This is opposed to using training data merely to select among different algorithms or using

heuristics/common sense to design an algorithm. Some commonly-used classification criterion includes: Bayesian decision theory, and Minimum-Error-Rate classification.

2. *Linear Discriminate Analysis*

Linear discriminate analysis (LDA) and the related Fisher linear discriminate are methods used in statistics, pattern recognition and machine learning to find a linear combination of features which characterizes or separates two or more classes of objects or events. The resulting combination may be used as a linear classifier, or more commonly, for dimension reduction before later classification. LDA is also closely related to principal component analysis (PCA) and factor analysis in that they both look for linear combinations of variables which best explain the data.

3. *Artificial Neural Network Classification*

An artificial neural network (ANN) is a mathematical model or computational model that is inspired by the structure and/or functional aspects of biological neural networks. A neural network consists of an interconnected group of artificial neurons, and it processes information using a connectionist approach to computation. In most cases an ANN is an adaptive system that changes its structure based on external or internal information that flows through the network during the learning phase. Modern neural networks are non-linear statistical data modeling tools. They are usually used to model complex relationships between inputs and outputs or to find patterns in data. In 2004,

Satoshi Kawai classified 3 human daily motions (lift up, put down, don't move) successfully by using EMG signals from human torso and a 3-layer ANN.

4. *Clustering Classification*

Clustering is the task of assigning a set of objects into groups (called clusters) so that the objects in the same cluster are more similar to each other than to those in other clusters. Clustering is a main task of explorative data mining, and a common technique for statistical data analysis used in many fields, including machine learning, pattern recognition, image analysis, information retrieval, and bioinformatics.

5. *Decision Tree Classification*

Decision tree classification, which used in statistics, data mining and machine learning, uses a decision tree as a predictive model which maps observations about an item to conclusions about the item's target value. In these tree structures, leaves represent class labels and branches represent conjunctions of features that lead to those class labels. There are many specific decision-tree algorithms. Notable ones such as: CART (classification and regression tree) algorithm, ID3 algorithm, C4.5 algorithm, CHi-squared Automatic Interaction Detector (CHAID) algorithm, which performs multi-level splits when computing classification trees and MARS (extends decision trees to better handle numerical data) algorithm.

In this project, decision trees were chosen to design the classifier since it is simple to understand and interpret, computational efficient to implement [49] and easy to

separate more than two classes of objects or events [48]. Training the classifier took only a few seconds, which is very important for real-time recognition system to ensure a fast response.

4.2 Details of Decision Tree Classification

Decision tree classification [50] is a kind of non-metric pattern recognition method for approximating discrete-valued target functions, in which the learned function is represented by a decision tree. The advantage of decision tree includes: simple to understand and interpret, have value even with little hard data, possible scenarios can be added, worst, best and expected values can be determined for different scenarios, use a white box model if a given result is provided by a model, and can be combined with other decision techniques. Disadvantage such as: output attribute must be categorical, limited to one output attribute, decision tree algorithms are unstable, and trees created from numeric datasets can be complex. Fig.15 shows a typical decision tree classifier. This decision tree classifies one day morning according to whether they are suitable for playing tennis. For example, the sample (Outlook =Rain, Temperature = Hot, Humidity = Normal, Wind =Weak) would be sorted down the right-most branch of this decision tree and would therefore be classified as a positive instance, that means PlayTennis = yes.
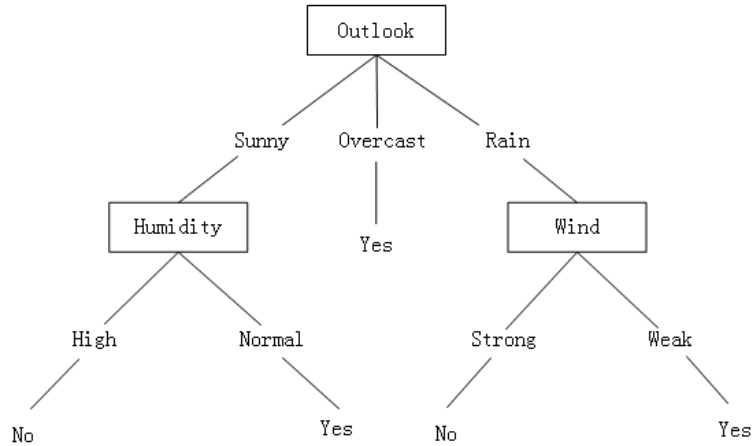
Figure 15. A typical decision tree for the concept of PlayTennis. [50]

Now comes to the question, how to create a decision tree based on training data? The basic generic tree-growing methodology know as CART (Classification and Regression Trees) algorithm, which provides a general framework that can be instantiated in various ways to produce different decision trees. The fundamental principle of tree creation is very simple: decisions that lead to a simple, compact tree with few nodes should be preferred [51]. This is a version of Occam's razor, that the simplest model that explains data is the one to be preferred. Therefore, a term called "impurity" should be defined in order to make sure the data reaching the immediate descendent nodes as pure as possible. Let $i(N)$ denotes the impurity of a node N. In all cases, $i(N)$ should be 0 if all of the patterns that reach the node bear the same category label, and to be large if the categories are equally represented. The most popular measure is the *entropy impurity*:

$$i(N) = -\sum_j P(\omega_j) \log_2 P(\omega_j) \tag{4.1}$$

where $P(\omega_j)$ is the fraction of patterns at node N that are in category ω_j.

The node entropy impurity is 0 if all the patterns are of the same category; otherwise it is positive, with the greatest value occurs when the different classes are equally likely. For example, suppose N is a collection of 14 examples of some boolean concept, including 5 positive and 9 negative examples. Then the entropy of N relative to this boolean classification is:

$$i(N) = -(9/14)\log_2(9/14) - (5/14)\log_2(5/14) = 0.94$$

Other impurity methods such as *Gini impurity*:

$$i(N) = 1 - \sum_j P^2(\omega_j) \tag{4.2}$$

This is just the expected error rate at node N if the category label is selected randomly from the class distribution present at N. This criterion is more strongly peaked at equal probabilities than entropy impurity.

And also *Misclassification impurity*:

$$i(N) = 1 - \max_j P(\omega_j) \tag{4.3}$$

This measure is the most strongly peaked at equal probabilities than the other two. Fig.16 shows these three impurity functions for a two-category case, as a function of the probability of one of the categories.
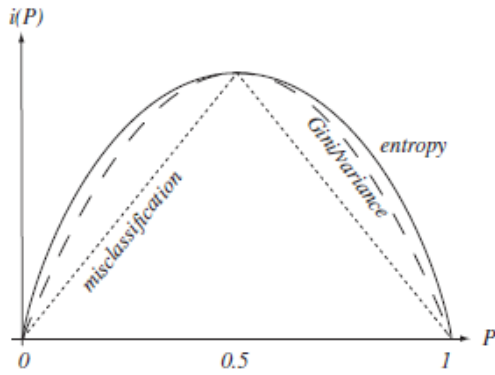
Figure 16. Three impurity functions for a two-category case. [51]

The CART algorithm learns decision trees by building them from top to down. Now comes to another important question: which attribute should we choose for the property test T at node N? One solution is to choose the test that decreases the impurity as much as possible. The information gain (drop in impurity) is defined by:

$$\Delta i(N) = i(N) - P_L i(N_L) - (1 - P_L) i(N_R) \qquad (4.4)$$

where NL and NR are the left and right descendent nodes, $i(NL)$ and $i(NR)$ their impurities, and PL is the fraction of patterns at node N that will go to NL when property test T is used. Therefore, the best test attribute is the choice for T that maximizes $\Delta i(N)$.

As mentioned before, decision trees were chosen to design the classifier in this project since it is computational efficiency to implement. So one may ask what is the time and space computational complexities of training the CART decision tree? To answer this question, suppose a two-category problem with n training patterns in d dimensions, and wish to build a binary tree based on entropy impurity. Therefore, the total average time

complexity is $O(dn (log\ n)^2)$. The space complexity is simply the number of nodes, which is $1 + 2 + 4 + ... + n/2 \approx n$, that is, $O(n)$.

In general, the tree won't stop growing until all of the nodes are pure. However, this will reflect the noise in the training data and the classifier can't perform well when applied to the unknown data. Fig.17 shows the impact of overfitting in decision tree learning. The horizontal axis indicates the total number of terminal nodes in the decision tree, as the tree is being constructed. The vertical axis indicates the classification accuracy rate made by each subtree. The solid line shows the accuracy rate by using resubstitution method, which is based on the training data that was used to create the original tree, whereas the broken line shows the accuracy rate by using 10-fold cross validation method. The accuracy rate of the tree measured by the resubstitution method increases monotonically. However, when measured by 10-fold cross validation method, the accuracy rate first increases, then decreases. As can be seen, once the tree size exceeds approximately 25 nodes, further elaboration of the tree decreases its accuracy rate over the test data despite increasing its accuracy rate on the training data. Therefore, it proves that the original decision tree overestimates the accuracy rate of applying the tree to new data.
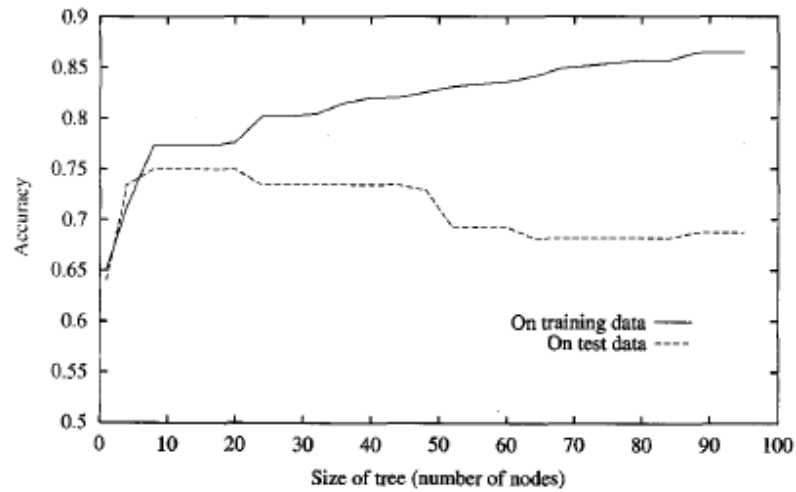
Figure 17. Impact of overfitting in decision tree learning. [50]

To avoid overfitting, a 10-fold cross validation (CV) method is utilized after training. In 10-fold cross validation, the function partitions the training data set (N samples) into ten subsets with $N/10$ each, choose randomly but with roughly equal size, nine subsets are used for training the classifier and the remaining one is used for testing. The procedure is then run ten times, each time using a different one of these subsets as the validation set and combining the other subsets for the training set. Thus, each subset is used in the validation set for one of the experiments and in the training set for the other 9 experiments. The mean classification accuracy rate is calculated as the performance metric for different number of terminal nodes of each subtree. Finally, the tree is pruned at the best level, which is the one that produces the smallest tree that is within one standard error of the maximum classification accuracy rate subtree. Fig.18 illustrates the effect of 10-fold cross validation pruning in decision tree learning. This plot shows the

36

same accuracy rate curves by using resubstitution and 10-fold cross validation methods. After pruning, the number of tree nodes is reduced, which lead to a strong generalization for unknown data and lower computational cost.
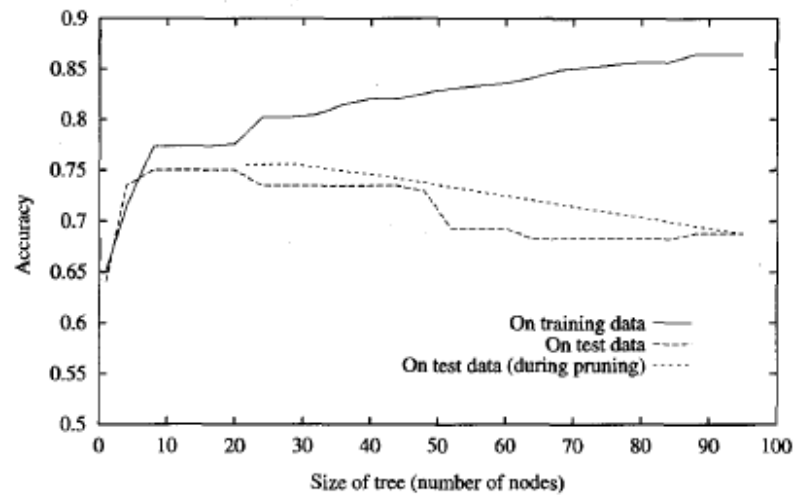
Figure 18. Effect of 10-fold cross validation pruning. [50]

While most tree-growing algorithms use entropy impurity criterion, there are many choices for stopping rules, for pruning methods and for the treatment of missing attributes, such as two other popular tree algorithms: ID3 and C4.5. In general, no single tree algorithm dominates or is dominated by others, which tree classifier to choose depends on certain situation.

CHAPTER 5

SURFACE ELECTROMYOGRAPHY AND INERTIAL SIGNALS BASED ACTIVITY MODE INTENT RECOGNITION

5.1 Introduction

The surface electromyography (sEMG) signals are detected over the skin surface and are generated by the electrical activity of muscle fibers during contraction. Multi-channel EMG signals, collected by electrodes placed on the involved muscles, can be used to identify the user's intent activity mode since each activity corresponds to a specific pattern of activation of several muscles. Therefore, sEMG signals are one of the major neural control sources for powered prostheses, exoskeleton and rehabilitation robots. Some prior works exist on developing sEMG pattern recognition-based control approach for many other kinds of powered prostheses, such as: A Gaussian mixture model based classification scheme for myoelectric control of powered upper limb prostheses is described in [41]. A volitional control approach of a prosthetic knee using surface electromyography is described in [42]. A multiclass real-time intent recognition method for a powered lower limb prosthesis is presented in [43]. Other researchers emphasize on describing the development of pattern recognition approach based on EMG signal, such as: An EMG-based pattern recognition approach for identifying locomotion

modes by using artificial neural networks (ANN) and linear discriminant analysis (LDA) is presented in [44]. A robust, real-time control scheme for multifunction myoelectric control is presented in [45]. An EMG-based hand gesture recognition approach for real-time biosignal interfacing is described in [46].

Current prosthetic devices predominantly utilize sEMG signals from the user's body, in addition to pressure and force sensors, mounted at various locations on the device and along the body. As part of efforts to develop a suitable sensor suite to recognize user intent, this chapter proposes an approach based on a combination of EMG and inertial sensors in order for sensor fusion. EMG signals from the user's body correspond to a local, area specific level, and play the most important role in pattern classification, while inertial sensors mounted on the exoskeleton and user correspond to a more holistic and generalized way of intent recognition. Related prior research works such as: A multimodal interpretation of muscular activities using a body sensor network with electromyogram and inertial sensors is developed in [47]. An automatic recognition method of sign language sub-words based on portable accelerometer and EMG sensors is described in [48]. A rule-based control approach of walking by using decision trees and practical sensors is designed in [49]. This chapter aims to describe a control structure which is safe, robust and reliable for the control of powered backbone exoskeleton, with the emphasis on developing activity mode intent recognizer.

5.2 Backbone exoskeleton control structure

5.2.1 Architecture

A three-level control structure for powered backbone exoskeleton is shown in Fig.19. It consists of a high-level supervisory controller, a middle-level controller and a low-level controller. The low-level controller is a closed-loop feedback controller which can control motor torques and compensate for the transmission dynamics. The middle-level controller generates torque references by using a finite-state machine which can regulate the impedance of the joints. The high-level controller consists of two parts: activity mode recognizer and state estimator. The state estimator is used to estimate actions of the user in order to trigger the corresponding middle-level controller. The activity mode recognizer distinguishes between different activity modes, such as flexion, extension and twisting. This project focuses on the activity mode recognizer and specifically describes the processing of EMG and inertial measurement unit (IMU) data streams and intent recognition algorithm by using decision tree.
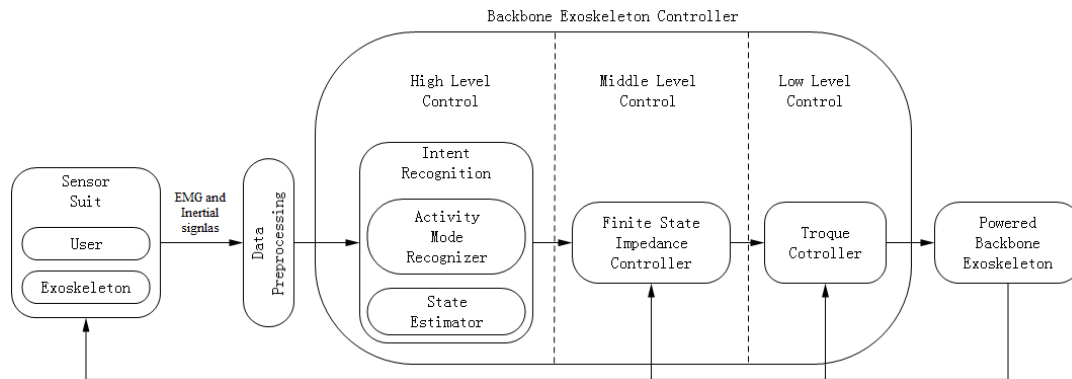
Figure 19. Powered backbone exoskeleton control structure.

5.2.2 Intent recognition methodology

Intent recognition, also called goal recognition, is the task of recognizing the intents of a subject by analyzing some or all of their actions and/or analyzing the changes in the state resulting from their actions based on certain classifier. The classifier was designed and trained with appropriate database in order to be used for real time intent recognition. Appropriate set of sensors, appropriate window length for sensor data streams, and appropriate set of features to extract from each window need to be determined in order to train and use the classifier. Further, an appropriate data dimension reduction method was needed for real-time implementation. After a decision tree classifier was established, it was used in real time to determine which activity was most probable at a certain instant in time. Finally, the result was essentially low-pass filtered by a majority voting system in order to filter out noise and increase classification accuracy. The specific procedure [43] is described below.

1. Sensor suite and data streams

The sensor suite for the backbone exoskeleton was designed for providing enough data streams for intent recognizer. It consists of EMG sensors on the flexor and extensor muscles of the back and abdomen, inertial measurement unit at multiple locations on the back to provide inertial measurement. The raw data streams were preprocessed by some

commonly used methods include: high-pass filtering, low-pass filtering, rectification and normalization

2. Feature selection and extraction

Features were selected from sliding windows in our project since a relatively long window can be condensed into few information-rich features. Both sliding disjoint and overlapped windows [45] were used in order to compare their classification accuracy rate and delay time respectively. The real-time nature of intent recognition system requires that the features selected should have low computational cost, such as mean absolute value or standard deviation. For each sensor channel, four features will be selected and then a feature space can be obtained after computing.

3. Dimension reduction

The feature space dimension needs to be reduced in order to keep the most important information, decrease the time requirement for training the classifier and facilitate the real-time system implementation. A previous research work on myoelectric pattern classification for upper limb prostheses [52] shows that principal component analysis (PCA) dimension reduction algorithm can fulfill the target successfully and also improve classification accuracy. So in this project PCA was considered for dimension reduction.

4. Decision tree classification

CART (classification and regression tree) was chose as the decision tree classifier [49]. It is computational efficiency to implement, training the classifier took only a few seconds, which is very important for real-time recognition system to ensure a fast response. The algorithm constructs the CART by making recursive binary splitting of the training data set. The data are partitioned into smaller and smaller subsets which are represented as the nodes in the tree until all of the nodes are pure. Gini impurity was used as split criterion:

$$i(N) = \sum_{i \neq j} P(\omega_i) P(\omega_j) = 1 - \sum_{j=1}^{k} P^2(\omega_j) \tag{4.5}$$

where $i(N)$ denote the impurity of a node N, $P(\omega_j)$ is the fraction of patterns at node N that are in category ω_j.

After training the binary decision tree, a 10-fold cross validation (CV) [50] method was utilized to prune the tree in order to avoid overfitting. Therefore, the classifier can show strong generalization when applied to the unknown data.

5. Majority voting system

The classification accuracy of the real-time intent recognizer can be increased by various kinds of low-pass filters. In this project we choose a majority voting system [41] which requires a majority agreement over a frame of activity mode decisions coming from the previous step in order to decide whether the high-level controller needs to switch activity mode or not. Such an approach can filter out noise and increase

classification accuracy, but at the cost of increased delay time. Thus the tradeoff between classification accuracy and switching latency based on certain requirement for an application should be estimated.

5.3   Implementation

5.3.1   Experimental design

An experimental study was designed to evaluate the performance of EMG and inertial measurement unit for providing enough data streams for intent recognizer. EMG signals were recorded by using a commercial EMG measurement system (DELSYS Myomonitor IV Wireless EMG System), while inertial signals were calculated from home-made inertial measurement unit board, as shown in Fig.20. The board includes: LIS331AL analog 3-axis 2G accelerometer with acceleration range: +/- 2g, sensitivity: 478.5mV/g, zero-g-level: 1.65V (+/- 6%) and low pass filter (noise reduction): 50Hz. LPR550AL dual-axis (Pitch and Roll) gyroscope and LY550ALH single axis (Yaw) gyroscope, each with measurement range: +/-500deg/sec, sensitivity: 2mV/Deg/sec, zero-rate level: 1.23V, high pass filter (drift compensation): 0.16Hz and low pass filter (noise reduction): 160Hz.

(a)   (b)

Figure 20. (a) Home-made Inertial Measurement Unit (IMU) board. (b) Connected to the QUALISYS motion capture systems by BNC connecter.

The EMG measurement system had 16 independent channels, each sampling at 1.2 kHz. Twelve of these channels were used and connected to Ag-AgCl (99.9% silver – silver chloride) surface EMG electrodes, with 10 mm spacing between the contacts. Eight electrodes were placed on the back and four were placed on the abdomen. The electrode mounting sites corresponded to multiple locations on the latissimus dorsi and erector spinae on the back, and the rectus abdominis and external obliques on the front, as shown in Fig.21. The inertial measurement unit system had two sensor boards with 6 independent channels each, 3 for inertial accelerometers and 3 for gyroscope sensors, each sampling at 1.2 kHz. Both of the two sensor boards were placed on the back. The two systems were synchronized in order to ensure a common time stamp on all the readings. A photograph of the placement of the sensor suite attached to the test subject is shown in Fig.22.
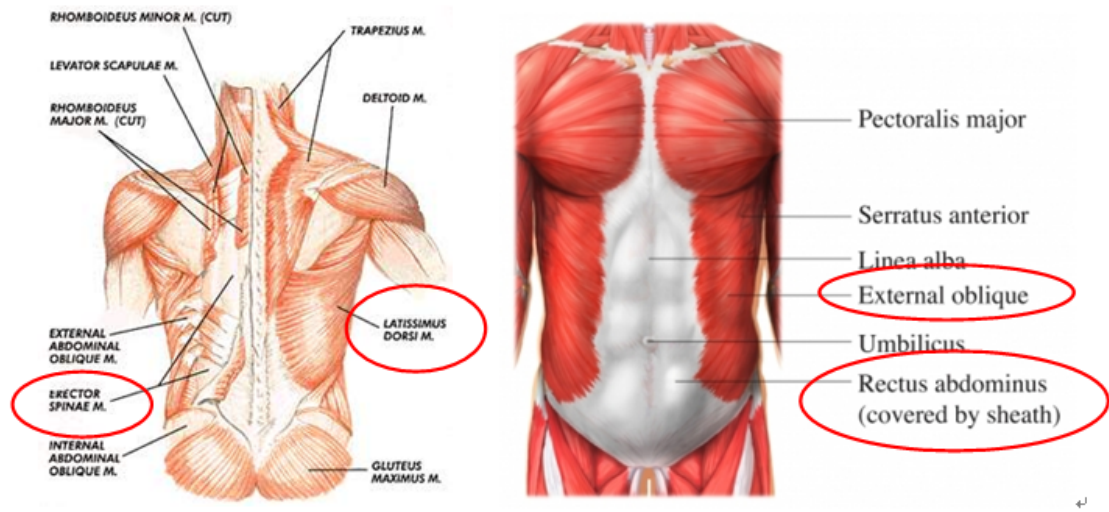
Figure 21. (a) Human back muscle. (b) Human front muscle. Red circles highlight muscles targeted in this study.
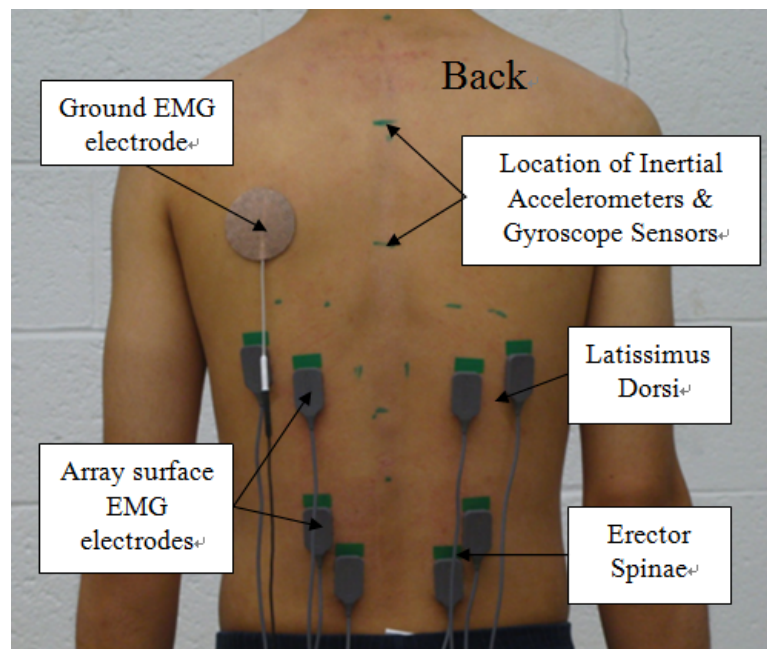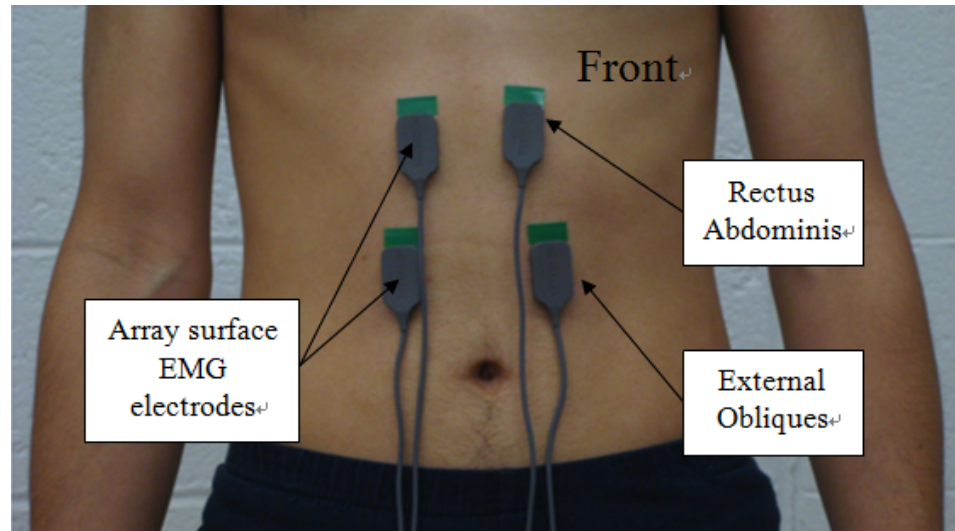
Figure 22. Placement of sensor suite (include EMG and Inertial Measurement Unit), subject: 30 year old healthy human with 1.83 m and 70 kg.

5.3.2　Test subject and experiment protocol

The testing protocol was approved by the Institutional Review Board at the University of Massachusetts, Amherst. The test subject were healthy individuals, 18 - 55 years old, free from any chronic pain, arthritis or any other disabilities and medical conditions. During the experiment, the subject spent approximately 2 hours at the biomechanics lab at UMass Amherst in the Kinesiology Department. sEMG sensors and inertial measurement units on the back and torso by using medical adhesives were placed on the subject. The subject was instructed to go through a series of daily motions such as flexion, extension twisting your torso, walking and running, as listed in Table 1 below. The speed of any motion was controlled by a device called Metronome, which keeps time

by beeping at a set interval, referred to a bpm (Beats per minute). For example, a metronome set at 60 bpm will beep or click at 60 beats per minute.

Activity	Time	Speed	Number of trails
Stand in neutral position	30 s	N/A	N/A
Twist torso left and back to neutral position	60 s	40 bpm	10
Twist torso right and back to neutral position	60 s	40 bpm	10
Stand in neutral position	30 s	N/A	N/A
Twist torso left and back to neutral position	60 s	60 bpm	15
Twist torso right and back to neutral position	60 s	60 bpm	15
Stand in neutral position	30 s	N/A	N/A
Flexion/Extension – Bend forward and stand back up	120 s	60 bpm	15
Flexion/Extension – Bend forward and stand back up	120 s	120 bpm	15
Stand in neutral position	30 s	N/A	N/A

Table 1. List of motions to be performed by subject during experiment.

5.3.3 Signal processing and analysis

The recorded raw sEMG signals were preprocessed by three steps [49]: First high-pass filtered by an 8thorder Butterworth filter with a 5 Hz cutoff frequency in order to remove any DC offset, minimize eventual movement artifacts. Then the signals were full-wave rectified and low-pass filtered by an 8th order Butterworth filter with a 20 Hz cutoff frequency to eliminate noise and interference in order to get a smooth signal, and also focus on the part of the spectrum during which large scale motion occurs [42] [53]. Dual-pass filter was used to get a zero-phase shift, thus the correct muscle activity timing

can be preserved. Finally, the signals were normalized in magnitude to the largest

amplitude observed during all the tests. Fig.23 shows a demonstration of preprocessing

result based on a subset of a raw sEMG signal, the signals were collected when test

subject twisted their torso left at the speed of 40 bpm. After preprocessing, the magnitude

of the signal in time domain was normalized between 0 and 1, the content of the signal in

frequency domain focused on the range of 5 – 20 Hz.
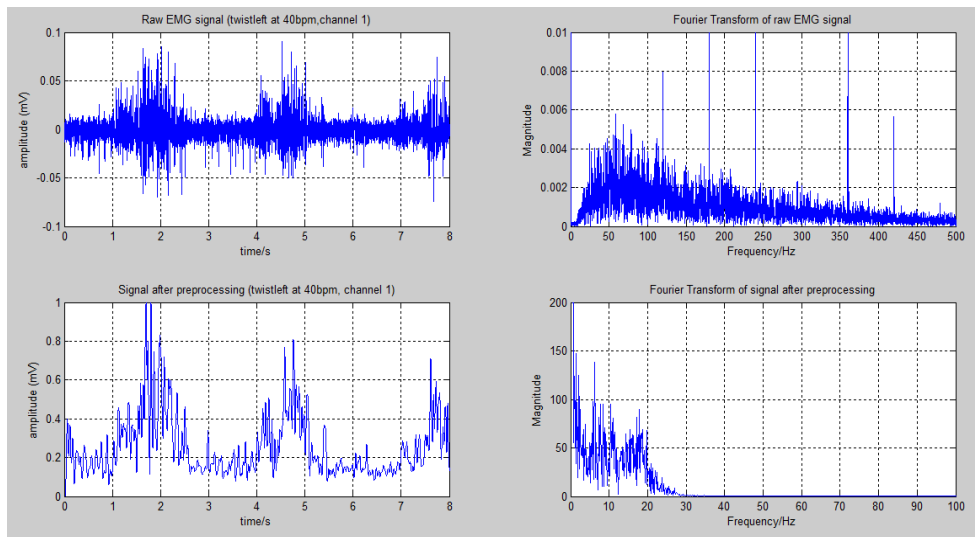
Figure 23. Demonstration of preprocessing result based on a subset of raw sEMG signal.

The signals from the inertial measurement unit were scaled to intervals [-1, 1],

Fig.24 shows sEMG and inertial signals recorded from the test subject after
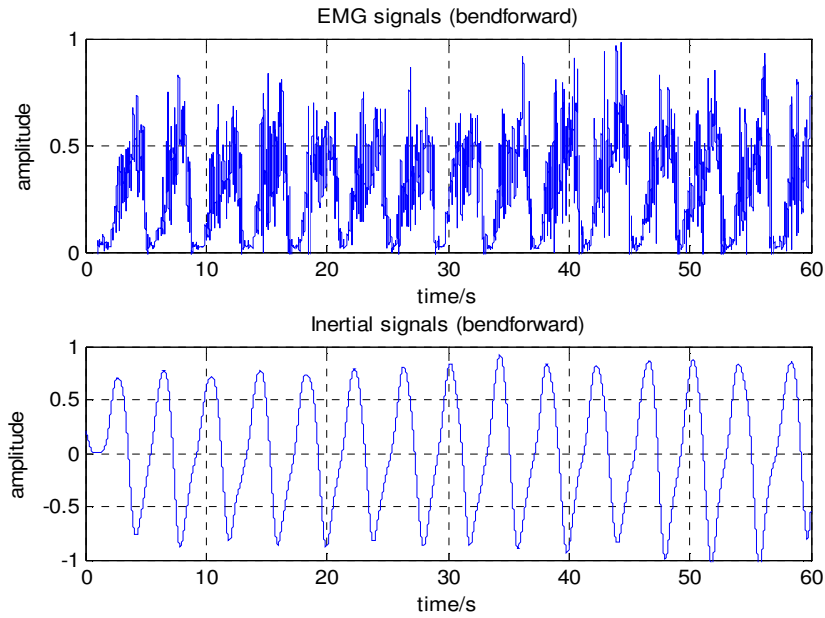
preprocessing.

Figure 24. sEMG and inertial signals recorded from the test subject after preprocessing.

After preprocessing, the database for each motion was split into two subsets, the training set and the test set. The first 60% of the trails were merged together for the training set and was used to generate classifier. The rest 40% of the trails were merged together for the test set and was used to validate the classifier generated by the training set. For example, the motion twist torso left and back to neutral position at the speed of 60 bpm had 15 trails, so the first 10 trails were merged together for training set and the rest 5 trails were merged together for test set.

Currently each motion had a 24-channel signal database, 12 for sEMG, 6 for inertial acceleration signal and 6 for gyroscope signal. Pattern classification was performed on sliding analysis window and the window length needed to be carefully considered. For such a real-time recognition system, the system delay time should not

perceivable by the user and the threshold is generally regarded to be about 300 ms [45], a long window length may challenge this constraint. Besides, the sEMG signal can be regarded as Gaussian random process [54], so the length of analysis window should not exceed 200 ms in order to ensure the small statistical variance of calculated features of EMG signals [44] since EMG signal plays the most important role in pattern classification. Therefore, the classification accuracy rate resulting from the window lengths ranging from 30 to 180 ms were compared [44] [55], for both sliding disjoint and overlapped window. Window increment for sliding overlapped window was decided to be 10 ms since the smaller the window increment, the faster the classification decision could be made. For each analysis window of each channel, four low computational cost features which could result in high classification accuracy rate [40] were computed, that include: mean absolute value (MAV), standard deviation (SD), difference absolute mean value (DAMV) and root mean square (RMS). Finally, each motion could get a 96-dimensional feature space after computing and PCA algorithm was used to reduce the dimension to three, these three principle components can represent most of the information of the original feature data set.

The three-dimensional training subset feature space of each motion was then provided to train decision tree classifier. In general, the tree wouldn't stop growing until all of the nodes are pure. However, this would reflect the noise in the training data and the classifier couldn't perform well when applied to the unknown data. Therefore, a

10-fold cross validation (CV) method was utilized to avoid overfitting after training. In 10-fold cross validation, the function partitioned the training data set (N samples) into ten subsets with $N/10$ each, chosen randomly but with roughly equal size, nine subsets were used for training the classifier and the remaining one was used for testing. The procedure was then run ten times, each time using a different one of these subsets as the validation set and combining the other subsets for the training set. Thus, each subset was used in the validation set for one of the experiments and in the training set for the other 9 experiments. The mean classification error rate was calculated as the performance metric for different number of terminal nodes of each subtree. Finally, the tree was pruned at the best level, which was the one that produces the smallest tree that was within one standard error of the minimum classification error rate subtree.

After pruning, the test subsets were provided to the decision tree classifier and then produced a decision stream. A majority voting postprocessing strategy was needed to filter out the noise and improve classification accuracy. In the majority voting postprocessing system, N classifier decisions were stored in a voting vector and the activity mode that occurs more than a certain *ratio* in those N decisions is selected as the high-level controller output. (For sliding disjoint window, N ranges from 10 to 60 in increments of 5, *ratio* equals to 60%. For sliding overlapped window, N ranges from 20 to 50 in increments of 5, *ratio* equals to 80%). The controller kept the previous output if none of the activity modes occur more than that ratio.

Delay time is very important for such a real-time control system. For example, Peleg et al. research work [56] performed classification results up to 1.4 seconds after the onset of the motion, which was perceivable and quite frustrating for the user. Therefore the delay time should be considered and discussed in details. Table 2 summarizes the equations for calculating delay time of different classifier type [57], while T_a represents the analysis window length, τ represents the processing time from the completion of data collection to a decision is made, T_{new} represents window increment of sliding overlapped window, n represents number of decisions in a voting vector. The whole signal processing system was performed on a 2.4-GHz Intel Core i3 based laptop with Maltab version of 32-bit R2010a.

Classifier type	Worst case delay	Average delay	Best case delay
No overlap, No majority voting	$D = \frac{3}{2}T_a + \tau$	$D = T_a + \tau$	$D = \frac{1}{2}T_a + \tau$
No overlap, With majority voting	$D = (\frac{n}{2}+1)T_a + \tau$	$D = (\frac{n+1}{2})T_a + \tau$	$D = (\frac{n}{2})T_a + \tau$
Overlap, No majority voting	$D = \frac{1}{2}T_a + T_{new} + \tau$	$D = \frac{1}{2}T_a + \frac{1}{2}T_{new} + \tau$	$D = \frac{1}{2}T_a + \tau$
Overlap, With majority voting	$D = \frac{1}{2}T_a + (\frac{n+1}{2})T_{new} + \tau$	$D = \frac{1}{2}T_a + (\frac{n}{2})T_{new} + \tau$	$D = \frac{1}{2}T_a + (\frac{n-1}{2})T_{new} + \tau$

Table 2. Delay time equations of different classifier type [57]

5.4 Results and discussions

5.4.1 10-fold cross validation pruning

Fig.25 (a) shows the impact of overfitting after training the decision tree. The horizontal axis indicates the total number of terminal nodes in the decision tree, as the

tree is being constructed. The vertical axis indicates the misclassification rate made by each subtree. The red line shows the misclassification rate by using resubstitution method, which is based on the same sample that was used to create the original tree, whereas the blue line shows the misclassification rate by using 10-fold cross validation method. As the figure shows, the misclassification rate of the tree measured by the resubstitution method decreases monotonically. However, when measured by 10-fold cross validation method, the misclassification rate first decreases, then increases. As can be seen, once the tree size exceeds approximately 40 nodes, further elaboration of the tree increases its misclassification rate over the new data despite decreasing its misclassification rate on the training data. Therefore, it proves that the original decision tree underestimates the misclassification rate of applying the tree to new data and the tree was pruned at the best level (showed in Fig.25 (a) by a purple circle), which is the one that produces the smallest tree that is within one standard error of the minimum misclassification rate subtree. Fig.25 (b) illustrates the effect of 10-fold cross validation pruning in decision tree learning. This plot shows the same misclassification rate curves by using resubstitution and 10-fold cross validation methods. After pruning, the number of tree nodes was reduced, which led to a strong generalization for unknown data and lower computational cost.
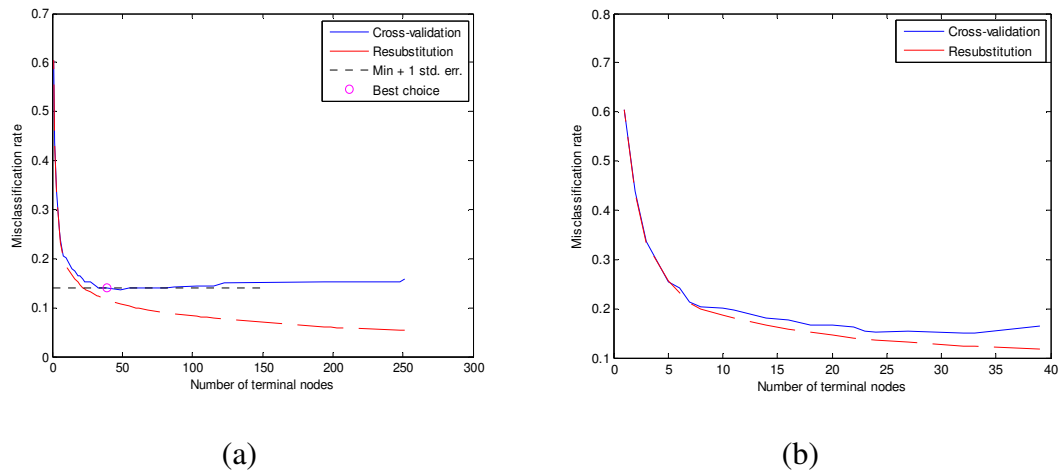
Figure 25. (a) Impact of overfitting and the best choice of number of terminal nodes (purple circle).   (b) Effect of 10-fold cross validation pruning.

5.4.2   Sliding disjoint window analysis

The decision tree classifier was finally built after pruning, then a 90-s long four-class motions (standing, twist torso left at 40 bpm, twist torso right at 40 bpm, bend forward at 60 bpm) test data trail was used to validate the performance of the classifier. Table 3 lists the recognition error rate (after majority voting) of different window length by using sliding disjoint window. For each window length, the recognition error rate was computed for different voting vector length ranged from 10 to 60 in increments of 5 and the one which resulted in the best recognition performance was chosen as the optimal length. As the table shows, the lowest recognition error rate is 0.43%, which corresponds to a window length of 100 ms and a voting vector length of 25. Fig.26 plots the

recognition error rate of different window length. The curve shows an overall upward

trend with fluctuation.

Window length (ms)	Voting vector length	Recognition error rate
30	25	2.97%
40	25	1.59%
50	40	0.49%
60	10	1.73%
70	25	6.87%
80	30	3.76%
90	20	2.89%
100	25	0.43%
110	15	2.38%
120	35	4.55%
130	60	3.19%
140	15	4.24%
150	15	8.29%
160	25	4.87%
170	15	5.00%
180	10	12.11%

Table 3. Recognition error rate of different window length by using sliding disjoint window, the shadow indicates the best recognition performance.
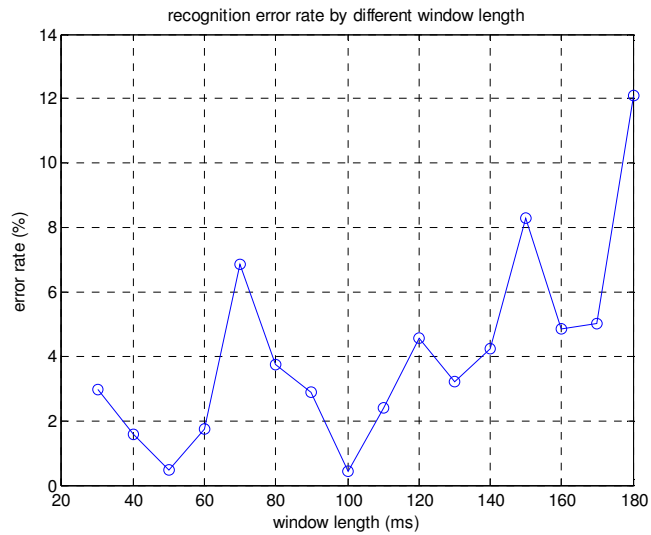
Figure 26. Recognition error rate of different window length (sliding disjoint window).

Fig.27 shows the output of the activity mode recognizer, using a window length of 100 ms and a voting vector length of 25. As can be seen, high recognition accuracy rate was achieved when comparing to the correct activity mode.

Figure 27. The output of the activity mode recognizer for a 90-s long test trial, with a window length of 100 ms and a voting vector length of 25.

After training and testing, the parameter of the classifier (window length and voting vector length) was fixed. Fig.28 shows a 120-s long real-time activity mode recognition result to test the performance of the classifier. During the experiment, the test subject was asked to do the same four-class motions, but with random order. The raw signal was then provided to the recognition system and the subject intent was outputted in real time. As can be seen, there is no obvious visual evidence of the incorrect switching except the switching latency, as the red broken line shows. The average delay time is:

$$\left(\frac{n+1}{2}\right)T_a + \tau = \frac{(25+1)}{2}*100 \, ms + 10 \, ms = 1310 \, ms = 1.3 \, s$$

which is far beyond the 300 ms maximum latency without a perceivable delay for the user.
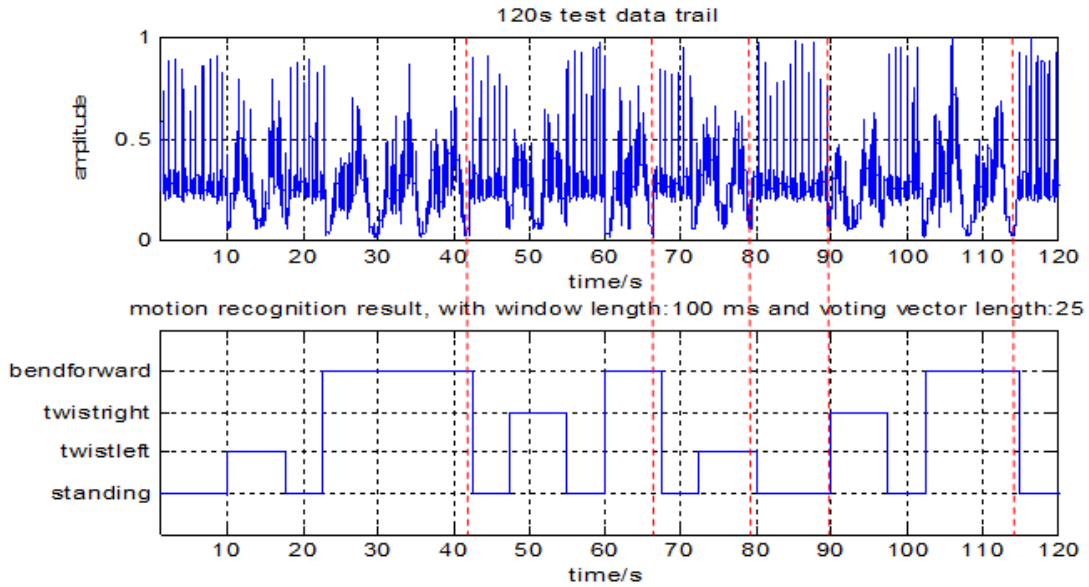
Figure 28. Real-time activity mode recognition for a 120-s long test trial.

5.4.3 Sliding overlapped window analysis

The processing (feature extraction and classification) only occurred in a portion of the time spent acquiring the raw signal when using sliding disjoint window, which indicated that the recognition system was underutilized, thus led to the unacceptable delay time. Another available approach was sliding overlapped window, which could fully utilize the computing capacity of the system and produce a decision stream as dense as possible. Table 4 lists the recognition error rate (after majority voting) of different

window length by providing the same test data trail to the classifier again. For each window length, the recognition error rate was computed for different voting vector length ranged from 20 to 50 in increments of 1 and the one which resulted in the best recognition performance was chosen as the optimal length. As the table shows, the lowest recognition error rate is 0.17%, which corresponds to a window length of 30 ms and a voting vector length of 38. Fig.29 plots the recognition error rate of different window length. The curve shows an overall upward trend with fluctuation, but the average error rate (1.84%) is much lower than using sliding disjoint window (4.10%).

Window length (ms)	Voting vector length	Recognition error rate
30	38	0.17%
40	43	1.16%
50	34	1.12%
60	29	2.22%
70	29	1.30%
80	35	2.17%
90	40	1.49%
100	46	2.30%
110	48	1.19%
120	42	2.48%
130	42	1.89%
140	48	2.20%
150	34	3.29%
160	50	3.24%
170	49	1.63%
180	42	2.60%

Table 4. Recognition error rate of different window length by using sliding overlapped window, the shadow indicates the best recognition performance.
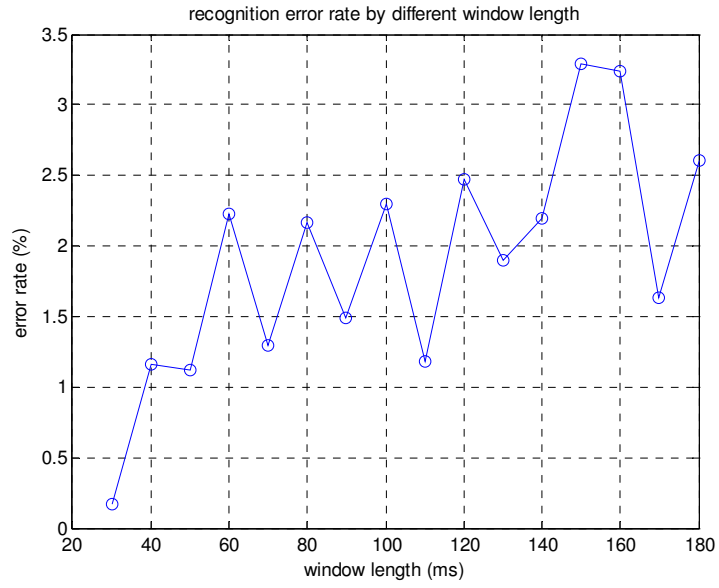
Figure 29. Recognition error rate of different window length (sliding overlapped window).

Fig.30 shows the output of the activity mode recognizer, using a window length of 30 ms and a voting vector length of 38. As can be seen, high recognition accuracy rate was achieved when comparing to the correct activity mode.
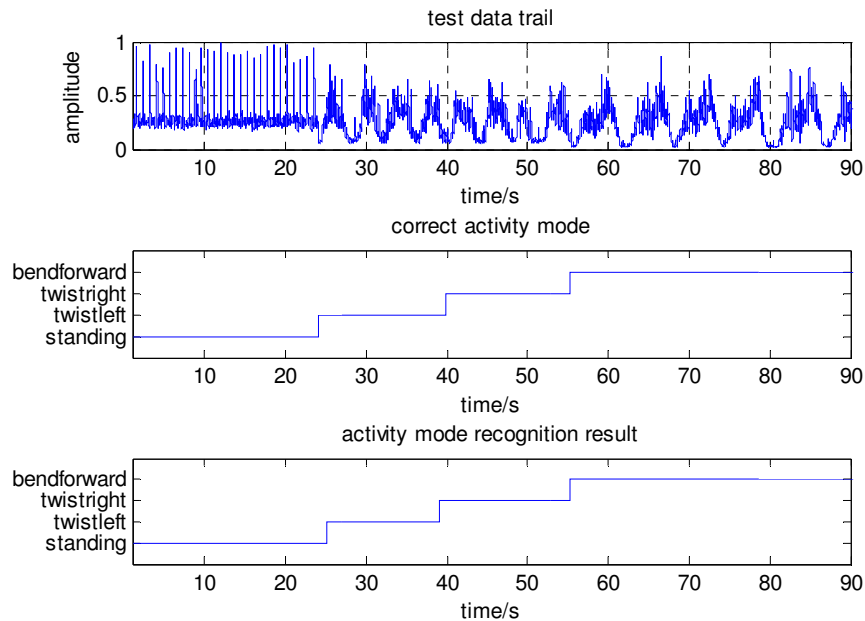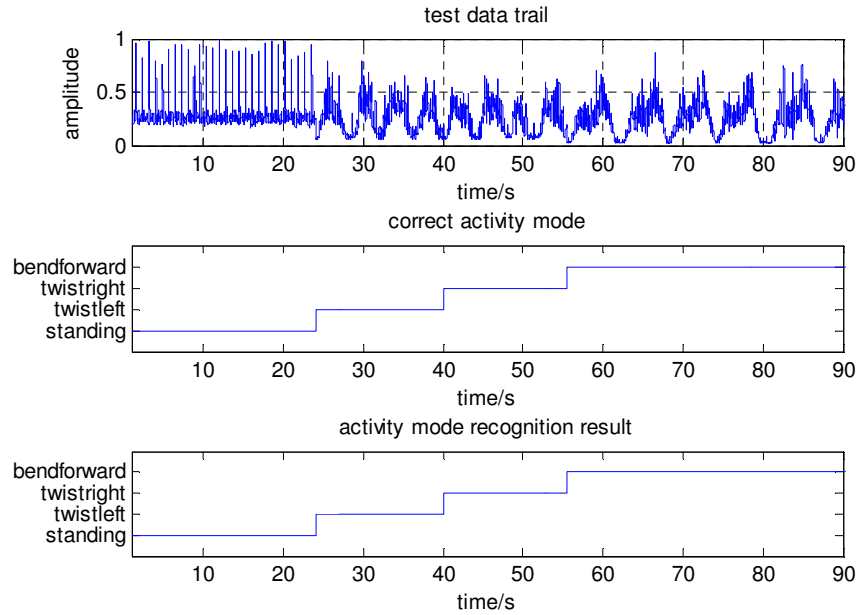
Figure 30. The output of the activity mode recognizer for a 90-s long test trial, with a window length of 30 ms and a voting vector length of 38.

After fixing the window length and voting vector length of the classifier, the same 120-s long data trail was used to test the performance of the classifier again, as the Fig.31 shows. Comparing to the recognition result by using sliding disjoint window, this approach shows no obvious visual evidence for both incorrect switching and the switching latency. The average delay time is:

$$\frac{1}{2}T_a + (\frac{n}{2})T_{new} + \tau = \frac{1}{2}*30\,ms + \frac{38}{2}*10\,ms + 10\,ms = 215\,ms$$

which is within the constraint and not perceived by the user. Therefore, an approach using sliding overlapped analysis window should be applied in order to generate faster decision updates, allow the system to be much more responsive, and ensure a high recognition accuracy rate system in mode switching.

61
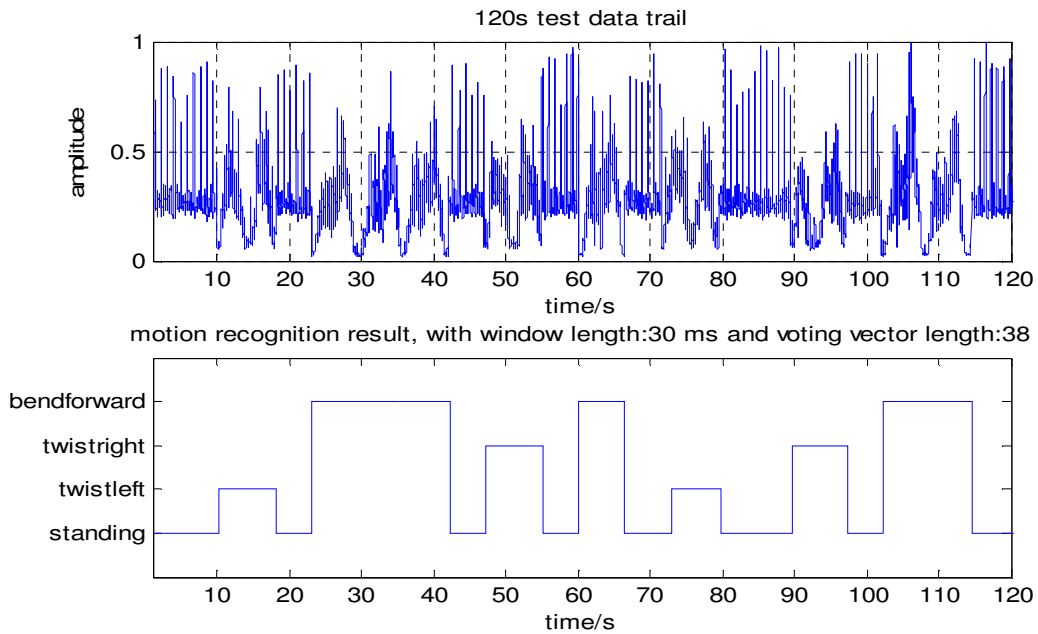
Figure 31. Real-time activity mode recognition for a 120-s long test trial.

5.4.4 Validating the performance of the recognizer via multiple subject dataset

To validate the performance of the intent recognizer using sliding overlapped window analysis four additional datasets were used from four different healthy subjects. Table 5 shows age, height and weight of each subject.

Subject	Age	Height (m)	Weight (kg)
2	34	1.93	83
3	25	1.70	60
4	29	1.81	72
5	26	1.75	66

Table 5. Age, height and weight of each subject.

Fig.32 plots the recognition error rate of different window length for all five subjects. All of these error rates show an overall increasing trend with variations, however, the minimum recognition error rate always occurred with window lengths between 30-50 ms. Therefore, for sliding overlapped window analysis, a smaller window length is better.
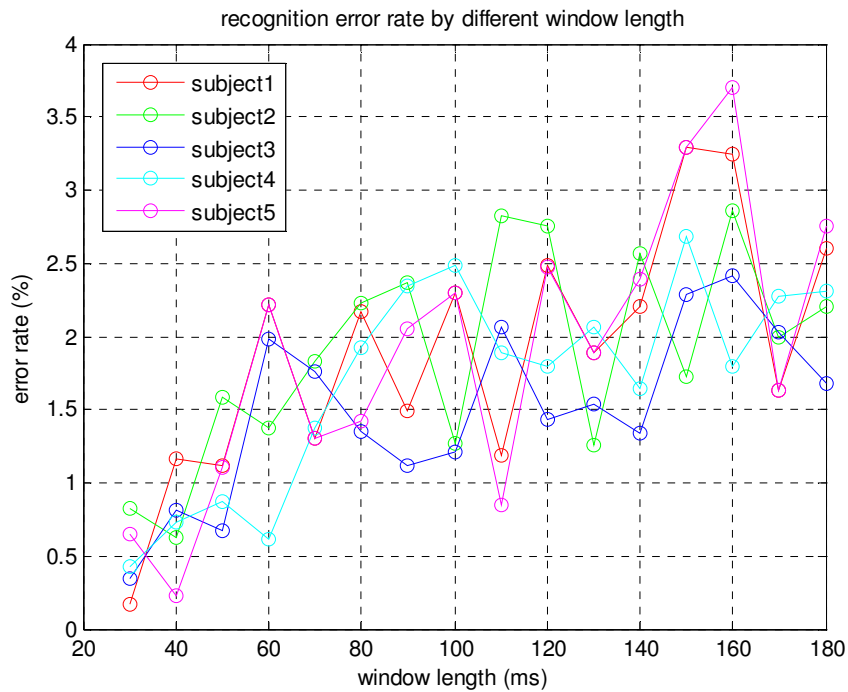
Figure 32. Recognition error rates for five subjects for different window lengths (sliding overlapped window).

Table 6 demonstrates the minimum recognition error rate and its corresponding window length and voting vector length for each test subject. From the table we can see that the optimal voting vector length which resulted in the best recognition performance of each subject focused on the range of 35 to 45, therefore a voting vector length which

belongs to this range could significantly eliminate misclassifications. All these five recognition error rates were below 1.00%, and the effective delay times were less than the 300 ms constraint. Therefore, the recognition results validate the performance of described recognizer with multiple subject datasets. The detailed recognition error rates results for the additional four subjects using different window lengths (similar to data shown for Subject 1 in Table 4) are presented in the Appendix. Also contained in the Appendix are the results of the 120 s real-time recognition tests for each of the additional subjects (as was shown for Subject 1 in Fig. 31).

Subject	Window length (ms)	Voting vector length	Recognition error rate	Delay time (ms)
1	30	38	0.17%	215
2	40	43	0.62%	245
3	30	36	0.35%	205
4	30	35	0.43%	200
5	40	41	0.23%	235

Table 6. Five subject test results (sliding overlapped window).

5.5   Conclusion

This chapter presents an activity mode intent recognizer, which is a high-level supervisory controller belongs to a three-level control structure for powered backbone exoskeleton. The recognizer uses surface electromyography and inertial signals as the input and CART (classification and regression tree) as the classifier. The CART algorithm is computational efficiency to implement, which is very important for real-time

recognition system to ensure a fast response. The approach was described in details and the experiment result indicates that the recognizer extracts the user intent and switches to the correct middle-level controller in real time. The approach achieves a low recognition error rate and a user-unperceived latency by using sliding overlapped analysis window, which shows great potential for implementing on a prototype backbone exoskeleton. Future study includes improving the recognition performance by incorporating additional sensors, adding new activity modes, such as twisting or bending at different speeds, walking and running, validating the performance of described recognizer with multiple subjects wearing a prototype backbone exoskeleton.

CHAPTER 6

CONCLUSIONS AND FUTURE STUDY

This thesis presents the development of an activity mode intent recognizer using surface electromyography and inertial measurement unit. The background and design concept of powered backbone exoskeleton, background of electromyography signal, and the necessary prerequisites for the thesis, namely the collection and processing of sEMG signal and the background of decision tree classification, were presented. The development of the activity mode intent recognizer was described which acts as a supervisory controller in a three-level control structure for a powered backbone exoskeleton. The recognizer uses surface electromyography and inertial signals as the input and CART (classification and regression tree) as the classifier. The experimental results indicate that the recognizer extracts the user intent in real-time. The approach achieves a low recognition error rate and is fast enough to potentially not be perceived by a user by using sliding overlapped analysis window. The approach shows great potential for implementing on a prototype backbone exoskeleton.

Future study includes improving the recognition performance by incorporating additional sensors, adding new activity modes, such as twisting or bending at different speeds, walking and running, validating the performance of described recognizer with multiple subjects wearing the prototype backbone exoskeleton, how this powered

backbone exoskeleton can be commercialized, and how the device can be used to restore

function for individuals with impairments (spinal cord injured) or coupled with lower and

upper limb robotic exoskeletons.

APPENDIX

FOUR TEST SUBJECTS RECOGNITION RESULTS

Tables 7-10 and Figures 33-36 in the appendix show the other four test subjects (Subject 2-5) recognition error rates of different window length and 120 s real-time recognition test results. The real-time recognition test results (Fig. 33-36) show no obvious visual evidence for both incorrect switching and the switching latency.

Window length (ms)	Voting vector length	Recognition error rate
30	48	0.83%
40	43	0.62%
50	37	1.59%
60	47	1.37%
70	29	1.83%
80	36	2.23%
90	47	2.37%
100	42	1.27%
110	45	2.83%
120	32	2.75%
130	42	1.26%
140	38	2.57%
150	34	1.73%
160	50	2.86%
170	45	1.99%
180	43	2.21%

Table 7. Subject 2 recognition error rate of different window length (sliding overlapped window), the shadow indicates the best recognition performance.

Figure 33. Subject 2 real-time activity mode recognition for a 120-s long test trial.

Window length (ms)	Voting vector length	Recognition error rate
30	36	0.35%
40	38	0.81%
50	43	0.67%
60	36	1.98%
70	34	1.76%
80	47	1.35%
90	37	1.12%
100	35	1.21%
110	42	2.07%
120	49	1.43%
130	46	1.54%
140	41	1.34%
150	38	2.29%
160	43	2.42%
170	39	2.03%
180	45	1.68%

Table 8. Subject 3 recognition error rate of different window length (sliding overlapped window), the shadow indicates the best recognition performance.

Figure 34. Subject 3 real-time activity mode recognition for a 120-s long test trial.

Window length (ms)	Voting vector length	Recognition error rate
30	35	0.43%
40	42	0.73%
50	32	0.87%
60	29	0.61%
70	37	1.38%
80	45	1.92%
90	34	2.35%
100	32	2.49%
110	38	1.89%
120	46	1.79%
130	47	2.07%
140	37	1.64%
150	46	2.68%
160	42	1.79%
170	45	2.27%
180	37	2.32%

Table 9. Subject 4 recognition error rate of different window length (sliding overlapped window), the shadow indicates the best recognition performance.
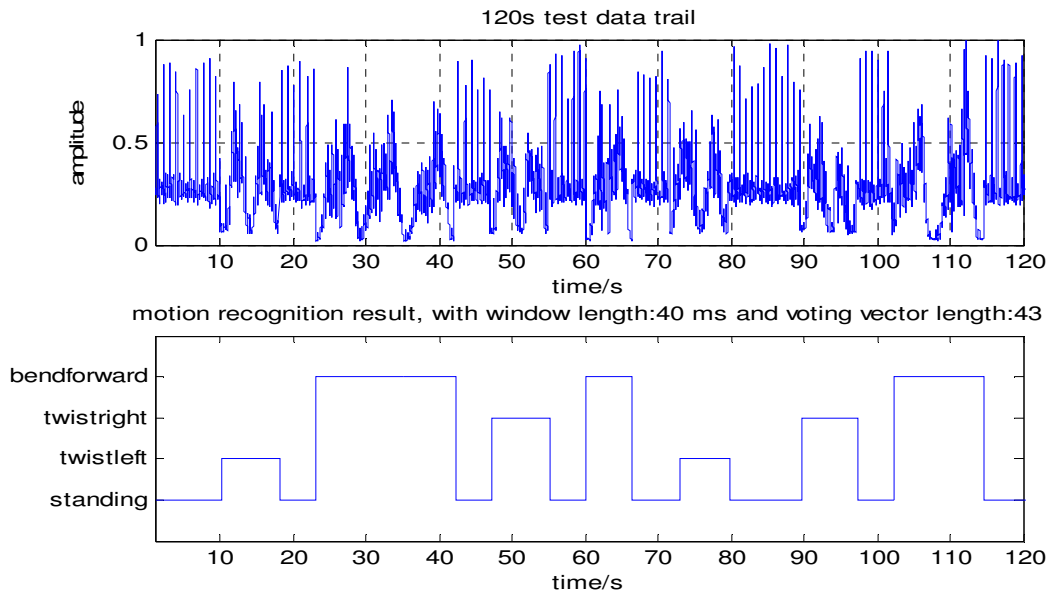
Figure 35. Subject 4 real-time activity mode recognition for a 120-s long test trial.

Window length (ms)	Voting vector length	Recognition error rate
30	43	0.65%
40	41	0.23%
50	34	1.11%
60	29	2.22%
70	29	1.30%
80	40	1.42%
90	29	2.05%
100	46	2.30%
110	38	0.85%
120	42	2.47%
130	42	1.89%
140	36	2.39%
150	34	3.29%
160	49	3.70%
170	49	1.63%
180	43	2.75%

Table 10. Subject 5 recognition error rate of different window length (sliding overlapped window), the shadow indicates the best recognition performance.
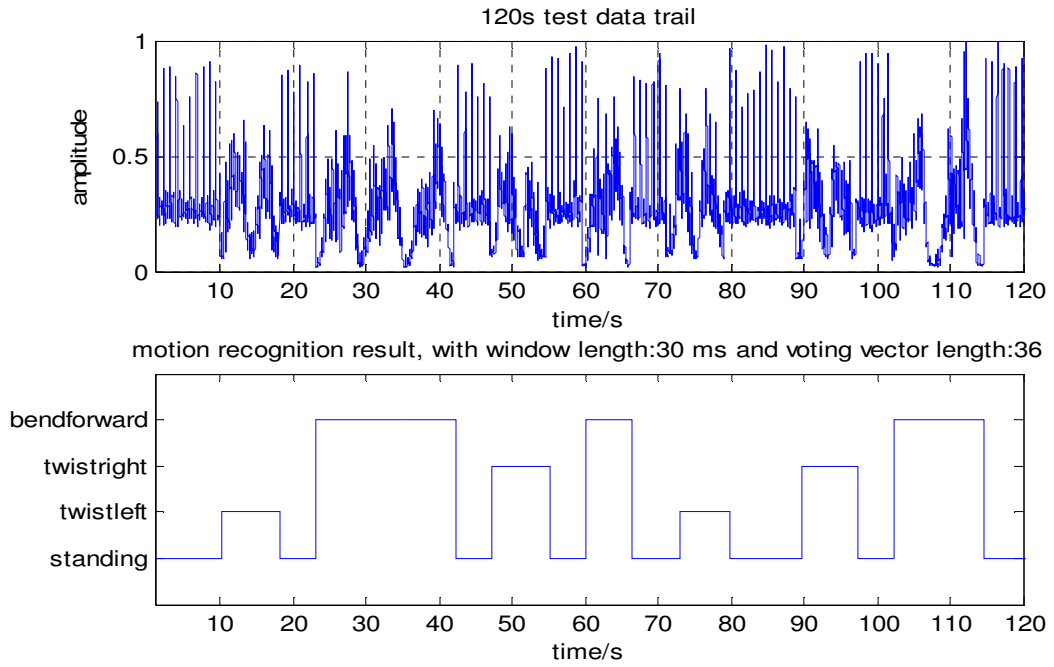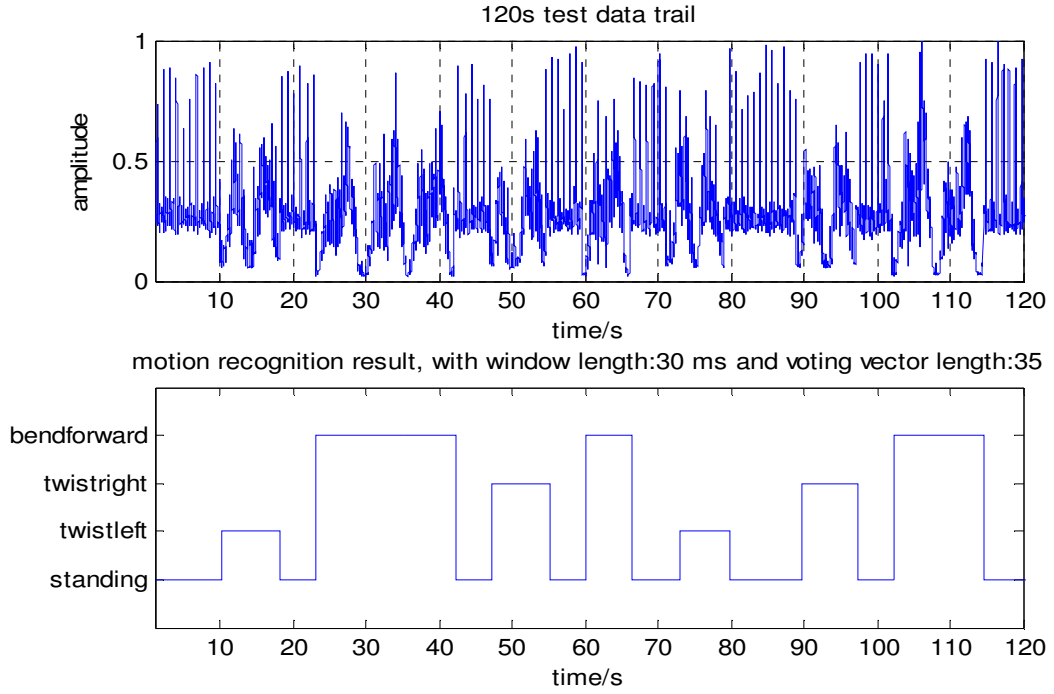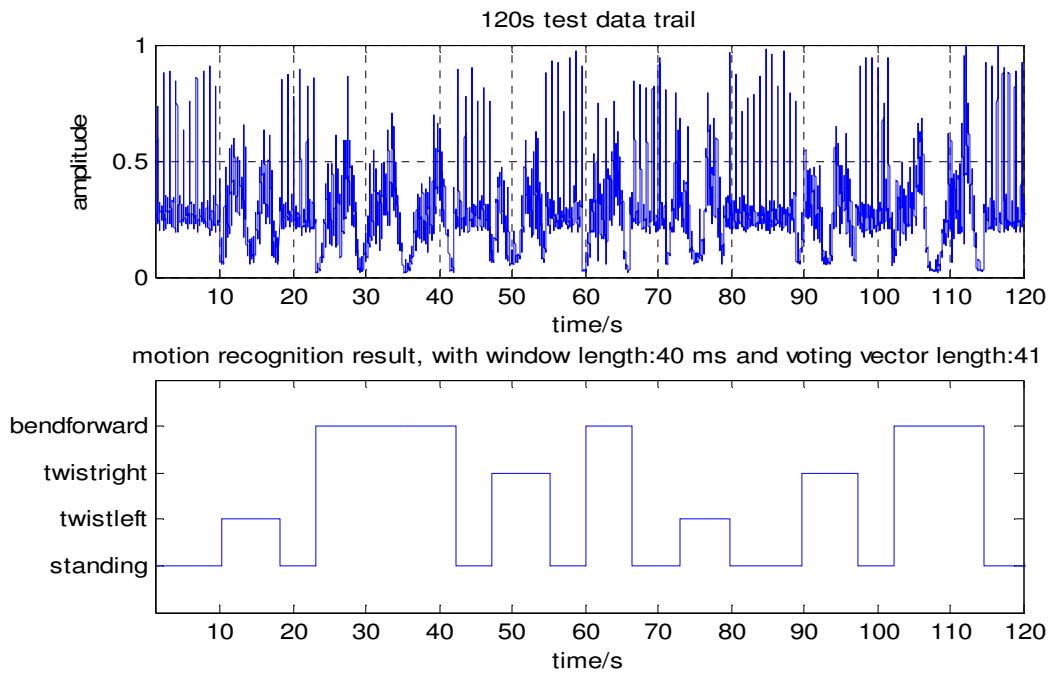
Figure 36. Subject 5 real-time activity mode recognition for a 120 -s long test trial.

BIBLIOGRAPHY

[1] H. Kazerooni, J. Racine, L. Huang, and R. Steger, "On the Control of the Berkeley Lower Extremity Exoskeleton (BLEEX)," *IEEE International Conference on Robotics and Automation*, pp. 4364–4371, 2005.

[2] E. E. Bleex, A. B. Zoss, H. Kazerooni, and A. Chu, "Biomechanical Design of the Berkeley Lower," *IEEE/ASME Tranctions on Mechatronics*, vol. 11, no. 2, pp. 128–138, 2006.

[3] C. J. Walsh, K. Endo, and H. Herr, "a Quasi-Passive Leg Exoskeleton for Load-Carrying Augmentation," *International Journal of Humanoid Robotics*, vol. 04, no. 03, pp. 487–506, 2007.

[4] H. Kawainot, S. Lee, S. Kanbe, and Y. Sankai, "Power Assist Method for HAL-3 using EMG-based Feedback Controller *," *IEEE International Conference on Systems, Man and Cybernetics*, pp. 1648–1653, 2003.

[5] H. Kawamoto and Y. Sankai, "Comfortable power assist control method for walking aid by HAL-3," *IEEE International Conference on Systems, Man and Cybernetics*, vol. 4, 2002.

[6] Y. Sankai, "Leading Edge of Cybernics: Robot Suit HAL," *2006 SICE-ICASE International Joint Conference*, vol. 10, p. P–1–P–2, 2006.

[7] S. C. Jacobsen, M. Olivier, F. M. Smith, D. F. Knutti, R. T. Johnson, G. E. Colvin, and W. B. Scroggin, "Research Robots for Applications in Artificial Intelligence, Teleoperation and Entertainment," *The International Journal of Robotics Research*, vol. 23, no. 4, pp. 319–330, Apr. 2004.

[8] S. Marcheschi, F. Salsedo, M. Fontana, and M. Bergamasco, "Body Extender: Whole body exoskeleton for human power augmentation," *2011 IEEE International Conference on Robotics and Automation*, pp. 611–616, May 2011.

[9] J. E. Pratt, B. T. Krupp, C. J. Morse, and S. H. Collins, "The RoboKnee   : An Exoskeleton for Enhancing Strength and Endurance During Walking," *IEEE International Conference on Robotics & Automation*, pp. 2430–2435, 2004.

[10]   R. J. Farris, H. a. Quintero, T. J. Withrow, and M. Goldfarb, "Design and simulation of a joint-coupled orthosis for regulating FES-aided gait," *2009 IEEE International Conference on Robotics and Automation*, pp. 1916–1922, May 2009.

[11]   S. Jezernik, G. Colombo, T. Keller, H. Frueh, and M. Morari, "Robotic orthosis lokomat: a rehabilitation and research tool.," *Neuromodulation : journal of the International Neuromodulation Society*, vol. 6, no. 2, pp. 108–115, Apr. 2003.

[12]   K. Naruse, "Development of Wearable Exoskeleton Power Assist System for Lower Back Support Yukinori K a k a," *IEEE/RSJ International Conference on Intelligent Robots and Systems*, pp. 3–8, 2003.

[13]   K. Naruse, S. Kawai, and T. Kukichi, "Three-dimensional lifting-up motion analysis for wearable power assist device of lower back support," *2005 IEEE/RSJ International Conference on Intelligent Robots and Systems*, pp. 2959–2964, 2005.

[14]   K. Yamamoto, M. Ishii, H. Noborisaka, and K. Hyodo, "Stand Alone Wearable Power Assisting Suit - Sensing and Control Systems -," *IEEE International Workshop on Robot and Human Interactive Communication*, pp. 661–666, 2004.

[15]   S. R. Taal and Y. Sankai, "Exoskeletal spine and shoulder girdle for full body exoskeletons with human versatility," *2011 IEEE International Conference on Robotics and Automation*, pp. 2217–2222, May 2011.

[16]   S. R. Taal and Y. Sankai, "Exoskeletal Spine and Shoulders for Full Body Exoskeletons in Health Care," *Advances in Applied Science Research*, vol. 2, no. 6, pp. 270–286, 2011.

[17]   H. Mochiyama, "Shape Control of Manipulators with Hyper Degrees of Freedom," *The International Journal of Robotics Research*, vol. 18, no. 6, pp. 584–600, Jun. 1999.

[18]   B. a. Jones and I. D. Walker, "Kinematics for multisection continuum robots," *IEEE Transactions on Robotics*, vol. 22, no. 1, pp. 43–55, Feb. 2006.

[19]   G. S. Chirikjian and J. W. Burdick, "A modal approach to hyper-redundant manipulator kinematics," *IEEE Transactions on Robotics and Automation*, vol. 10, no. 3, pp. 343–354, Jun. 1994.

[20] I. A. Gravagne, C. D. Rahn, I. D. Walker, and S. Member, "Planar Continuum Robots," *IEEE/ASME Transactions on Mechatronics*, vol. 8, no. 2, pp. 299–307, 2003.

[21] S. K. Dwivedy and P. Eberhard, "Dynamic analysis of flexible manipulators, a literature review," *Mechanism and Machine Theory*, vol. 41, no. 7, pp. 749–777, Jul. 2006.

[22] H. Mochiyama, "Hyper-flexible robotic manipulators," *IEEE International Symposium on Micro-NanoMechatronics and Human Science*, pp. 41–46, 2005.

[23] F. Manipulator, "Frenet-Serret Manipulator," *IEEE/ASME International Conference on Advanced Intelligent Mechatronics Proceedings*, vol. 3, no. 7, pp. 20–25, 2001.

[24] M. Ogle, "Anatomy of the Spine," *About.com*, 2010. [Online]. Available: http://pilates.about.com/od/technique/ss/human-spine-anatomy.htm.

[25] G. Feng, "Initialization Methods for an EMG-based Silent Speech Recognizer," *Master Thesis*, 2010.

[26] V. Medved, *Measurement of Human Locomotion*. Boca Raton, FL: CRC Press, 2000.

[27] J. R. Cram, "The history of surface electromyography.," *Applied psychophysiology and biofeedback*, vol. 28, no. 2, pp. 81–91, Jun. 2003.

[28] J.V. Basmajian, "Muscles alive: Their functions revealed by electromyography.pdf," *Journal of Medical Education*, vol. 37, no. 8, 1962.

[29] G. S. J.V. Basmajian, "A new bipolar electrode for electromyography.pdf," *Journal of Applied Physiology*, p. 849, 1962.

[30] J. R. Cram and J. C. Steger, "EMG scanning in the diagnosis of chronic pain," *Biofeedback and self-regulation*, vol. 8, no. 2, pp. 229–241, Jun. 1983.

[31] C. Luca, "The Use of Surface Electromyography in Biomechanics.pdf," *Journal of Applied Biomechanics*, vol. 13, pp. 135–163, 1997.

[32] "Structure of Skeletal Muscle," *National Cancer Institute*. [Online]. Available: http://training.seer.cancer.gov/anatomy/muscular/structure.html.

[33] N. Shapiro, "Motor Unit Recruitment Strategies During Deep Muscle Pain," *The Alchemist*, 2009. [Online]. Available: http://natchem.wordpress.com/2009/11/23/motor-unit-recruitment-strategies-durin g-deep-muscle-pain/.

[34] E. Z. De Luca CJ, "Common drive of motor units in regulation of muscle force," *Trends in Neuroscience*, vol. 17, pp. 299–305, 1994.

[35] L. J. Hargrove, K. Englehart, and B. Hudgins, "A comparison of surface and intramuscular myoelectric signal classification.," *IEEE transactions on bio-medical engineering*, vol. 54, no. 5, pp. 847–853, May 2007.

[36] Delsys, "DELSYS Myomonitor IV EMG System User's Guide." 2009.

[37] MarkusB, "6DOF robot arm controlled by speech recognition or EMG," *letsmakerobots.com*, 2011. [Online]. Available: http://letsmakerobots.com/node/25919.

[38] M. A. Oskoei and H. Hu, "GA-based Feature Subset Selection for Myoelectric Classification," *2006 IEEE International Conference on Robotics and Biomimetics*, pp. 1465–1470, 2006.

[39] S. H. Park and S. P. Lee, "EMG pattern recognition based on artificial intelligence techniques.," *IEEE transactions on rehabilitation engineering : a publication of the IEEE Engineering in Medicine and Biology Society*, vol. 6, no. 4, pp. 400–405, Dec. 1998.

[40] R. Boostani and M. H. Moradi, "Evaluation of the forearm EMG signal features for the control of a prosthetic hand.," *Physiological measurement*, vol. 24, no. 2, pp. 309–319, May 2003.

[41] Y. Huang, K. B. Englehart, S. Member, B. Hudgins, and A. D. C. Chan, "A Gaussian Mixture Model Baesd Classification Scheme for Myoelectric Control of Powered Upper Limb Prostheses," *IEEE Transactions on Biomedical Engineering*, vol. 52, no. 11, pp. 1801–1811, 2005.

[42] K. H. Ha, H. A. Varol, and M. Goldfarb, "Volitional control of a prosthetic knee using surface electromyography.," *IEEE transactions on bio-medical engineering*, vol. 58, no. 1, pp. 144–151, Jan. 2011.

[43]   H. A. Varol, F. Sup, and M. Goldfarb, "Multiclass real-time intent recognition of a powered lower limb prosthesis.," *IEEE transactions on bio-medical engineering*, vol. 57, no. 3, pp. 542–551, Mar. 2010.

[44]   H. Huang, T. A. Kuiken, S. Member, and R. D. Lipschutz, "A Strategy for Identifying Locomotion Modes Using Surface Electromyography," *IEEE Transactions on Biomedical Engineering*, vol. 56, no. 1, pp. 65–73, 2009.

[45]   K. Englehart and B. Hudgins, "A robust, real-time control scheme for multifunction myoelectric control.," *IEEE transactions on bio-medical engineering*, vol. 50, no. 7, pp. 848–54, Jul. 2003.

[46]   J. Kim, S. Mastnik, and E. André, "EMG-based hand gesture recognition for realtime biosignal interfacing," *Proceedings of the 13th international conference on Intelligent user interfaces - IUI   '08*, pp. 30–39, 2008.

[47]   H. Ghasemzadeh, R. Jafari, and B. Prabhakaran, "A body sensor network with electromyogram and inertial sensors: multimodal interpretation of muscular activities.," *IEEE transactions on information technology in biomedicine : a publication of the IEEE Engineering in Medicine and Biology Society*, vol. 14, no. 2, pp. 198–206, Mar. 2010.

[48]   Y. Li, X. Chen, J. Tian, X. Zhang, K. Wang, and J. Yang, "Automatic recognition of sign language subwords based on portable accelerometer and EMG sensors," *International Conference on Multimodal Interfaces and the Workshop on Machine Learning for Multimodal Interaction on - ICMI-MLMI   '10*, 2010.

[49]   S. Dosen, S. Member, and D. B. Popovic, "Rule-based Control of Walking by Using Decision Trees and Practical Sensors," *9th Symposium on Neural Network Applications in Electrical Engineering*, 2008.

[50]   T. M. Mitchell, *Machine Learning*. New York: McGraw-Hill, 1997.

[51]   D. G. S. R. O. Duda, P. E. Hart, *Pattern Classification*. Wiley, 2001.

[52]   L. J. Hargrove, G. Li, K. B. Englehart, and B. S. Hudgins, "Principal components analysis preprocessing for improved classification accuracies in pattern-recognition-based myoelectric control.," *IEEE transactions on bio-medical engineering*, vol. 56, no. 5, pp. 1407–1414, May 2009.

[53] G. K. and D. Gabriel, *Essentials of Electromyography*. Champaign, IL: Human Kinetics, 2010.

[54] B. Hudgins, P. Parker, and R. N. Scott, "A new strategy for multifunction myoelectric control.," *IEEE transactions on bio-medical engineering*, vol. 40, no. 1, pp. 82–94, Jan. 1993.

[55] L. H. Smith, L. J. Hargrove, B. a Lock, and T. a Kuiken, "Determining the optimal window length for pattern recognition-based myoelectric control: balancing the competing effects of classification error and controller delay.," *IEEE transactions on neural systems and rehabilitation engineering: a publication of the IEEE Engineering in Medicine and Biology Society*, vol. 19, no. 2, pp. 186–192, Apr. 2011.

[56] D. Peleg, E. Braiman, E. Yom-Tov, and G. F. Inbar, "Classification of finger activation for use in a robotic prosthesis arm.," *IEEE transactions on neural systems and rehabilitation engineering: a publication of the IEEE Engineering in Medicine and Biology Society*, vol. 10, no. 4, pp. 290–293, Dec. 2002.

[57] T. R. Farrell, "Determining delay created by multifunctional prosthesis controllers.," *Journal of rehabilitation research and development*, vol. 48, no. 6, Jan. 2011.